ELSEVIER

Tectonophysics 346 (2002) 247–275

TECTONOPHYSICS

www.elsevier.com/locate/tecto

The Migif–Hafafit gneissic complex of the Egyptian Eastern Desert: fold interference patterns involving multiply deformed sheath folds

Abdel-Rahman Fowler [a,*], Baher El Kalioubi [b]

[a] *Geology Department, Faculty of Science, United Arab Emirates University, P.O. Box 17551 Al-Ain, Abu Dhabi, United Arab Emirates*
[b] *Geology Department, Ain Shams University, Abbassiya, Cairo, Egypt*

Received 27 October 2000; accepted 22 October 2001

Abstract

The Wadi Hafafit Complex (WHC) is an arcuate belt of orthogneisses, migmatites and other high-grade metamorphic rocks, which marks the boundary between the Central Eastern and the South Eastern Deserts of Egypt. In the WHC, gneissic meta-gabbro outlines macroscopic fold interference patterns characterized by elliptical to irregular culminations cored by gneissic meta-tonalite to meta-trondhjemite. The five main culminations of the WHC have previously been labeled A (most northerly), B, C, D and E (most southerly). A detailed structural investigation of B, C, D and E reveals that these structures are a result of the interference of four macroscopic fold phases, the first three of which may represent a single deformation event. The first folding involved sheath-like fold nappes, which were transported to the N or NW, assisted by translation on gently dipping mylonite zones. The regional gneissosity and mineral extension lineations formed during this folding event. The fold nappes were deformed by mainly open upright small macroscopic and mesocopic folds with approximately NE-trending hinges. As a probable continuation of the latter folding, the sheaths were buckled into large macroscopic folds and monoclines with the same NE-trends. The fourth macroscopic folding resulted from shortening along the NE–SW direction, producing mainly NW–SE-trending upright gently plunging folds. Gravitative uplift is disputed as a component of the deformation history of the WHC. The peculiarities of the fold interference pattern result from the interesting behaviour of sheath folds during their refolding.
© 2002 Elsevier Science B.V. All rights reserved.

Keywords: Sheath folds; Fold interference patterns; Multiple folding; Migif–Hafafit gneisses; Egyptian Eastern Desert; Pan-African geology

1. Introduction

The Wadi Hafafit Complex (WHC) (El Ramly and Akaad, 1960; El Ramly and Saleeb Roufaiel, 1974; El Ramly et al., 1984; Greiling et al., 1988) represents the central part of a broader approximately E–W-trending arcuate zone of medium-grade gneisses (the Migif–Hafafit Gneisses), spanning almost the entire width of the Pan-African basement exposures in the Eastern Desert of Egypt (Fig. 1). The WHC is bounded to the north by a major north-convex thrust (the Nugrus Thrust) (Greiling et al., 1988; El Ramly et al., 1993) (Fig. 1), a thick mylonitic shear zone, which separates the high-temperature metamorphic rocks of the WHC (tier 1 of Bennett and Mosley, 1987) from mainly low-grade metamorphic ophiolitic and arc volcanic assemb-

* Corresponding author. Fax: +971-37671291.
E-mail address: tomabdurahman@hotmail.com (A.-R. Fowler).

0040-1951/02/$ - see front matter © 2002 Elsevier Science B.V. All rights reserved.
PII: S0040-1951(01)00259-1

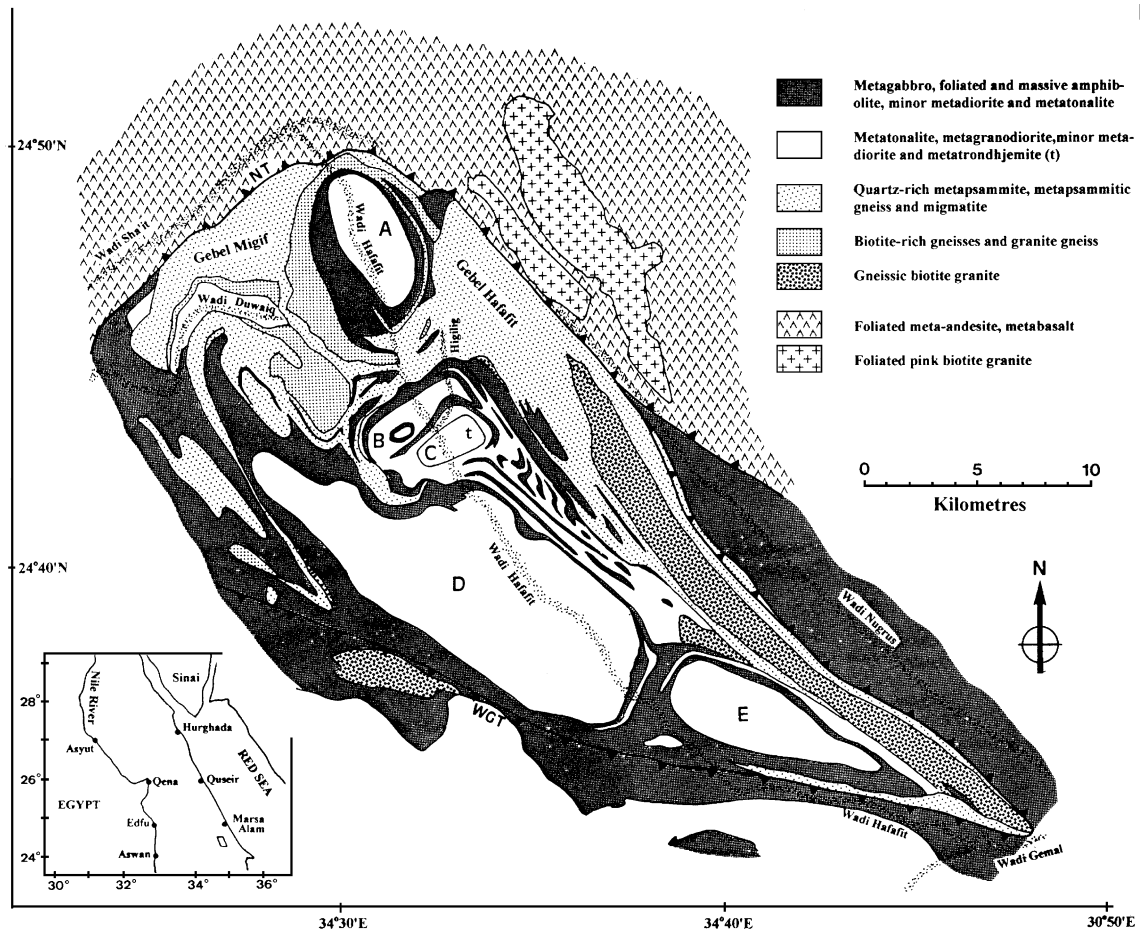

Fig. 1. Location and lithological map of the Wadi Hafafit Culmination, SSW of Marsa Alam, Egypt (modified from El Ramly and Greiling, 1988). Fold interference dome structures are labeled A to E. The structure of the area surrounding domes B, C, D and E is represented in Fig. 4. The Wadi Hafafit Culmination is bordered to the north by the Nugrus Thrust (NT), and to the south by the Wadi Gemal Thrust (WGT).

lages of the Central Eastern Desert (tier 2). The WHC is limited to the southwest, south and northeast by the folded Wadi Gemal Thrust (Greiling, 1997) (Fig. 1). The mafic orthogneisses and quartz-rich paragneisses and migmatites of the WHC enclose a set of peculiarly shaped granitoid gneiss-cored macroscopic dome structures (El Ramly and Akaad, 1960) (Fig. 1), labeled A to E, from north to south.

The Migif–Hafafit Gneisses have been regarded as pre-Pan-African remobilized crystalline basement by some authors (e.g. El Gaby et al., 1984, 1988), and as Pan-African age volcanic arc-related mafic lavas and granitoids by others (e.g. Rashwan, 1991; Kröner et al., 1994). Radiometric dating of zircons has firmly supported the second proposition (Hedge et al., 1982; Kröner et al., 1988, 1994), and geochemical analyses also confirm the similarity between these gneisses and the lower grade Pan-African assemblages above them (Rashwan, 1991; El Ramly et al., 1993). Another approach to determining the tectonic relations between the tier 1 gneisses and the overlying low-grade tier 2 assemblages is to compare their structural histories, especially the sequence of deformation events and their respective kinematics.

The aim of this work is to provide an overall model for the structural evolution of the WHC, from which future comparisons of tier 1 and tier 2 structure may be discussed in a tectonic context. An important

stage in this process is the resolution of the problem of the peculiar fold interference patterns shown by the WHC gneisses. Earlier attempts at analysis have suggested that late gravitative uprising of the cores of the domes caused distortion of the interference pattern (Greiling et al., 1984; El Ramly et al., 1984). Several models have been advanced to explain the patterns in terms of complex fault–bend folding (Greiling et al., 1988, 1996; Greiling, 1997). We have approached this problem from the reasoning that the peculiar interference pattern may rather reflect the unusual style of one or more of the fold generations. In particular, we have found that the first macroscopic folds show evidence for a strongly non-cylindrical geometry consistent with curved hinge folds or sheath folds.

After brief descriptions of the lithologies of the WHC, and the outcrop scale structures, we present the evidence for the existence of a first generation of macroscopic folds with sheath-like geometry. The existence and difficulty of recognition of macroscopic sheath folds have been discussed by Rhodes and Gayer (1977), Henderson (1981), Lacassin and Mattauer (1985) and Goscombe (1991). The individual elements of the WHC fold interference pattern are analyzed in terms of an early sheath fold model and some conclusions regarding controls on the styles of refolding of sheaths are presented. The evidence for gravitative uplift and fault–bend folding in the generation of these patterns is then critically reviewed.

2. Lithological units

2.1. Massive meta-gabbro

Very coarse-grained (up to 1-cm grain-size) blackish meta-gabbros occur as blocks, lenses and boudins usually within more abundant foliated meta-gabbros, e.g. elongate blocks and folded boudins to the east and south of dome C. The massive lithologies preserve much of the original texture of their gabbroic parent, which consisted originally of calcic plagioclase, clinopyroxene, olivine and titaniferous opaques. Some of the pyroxene, olivine and opaques remain but are mantled by concentric bands of metamorphic phases including pale green and colourless amphiboles and garnet (which enclose the relict pyroxenes and olivine), and brownish hornblende (which encloses the opaques).

2.2. Foliated meta-gabbro

These are the dominant lithologies surrounding the dome structures of the WHC. They are blackish rocks including varieties with distinct gneissic banding (hornblende gneiss) and others with penetrative foliation but no banding (amphibolites). Gneissosity is defined by hornblende-rich and plagioclase-rich alternating bands. The microstructure of the gneissosity and other foliations for all lithologies is described below. The foliated gabbros are typically coarse-grained (0.65–1.00-mm average grain-size range) and composed usually of >50% olive green subhedral hornblende grains and at least 40% poorly twinned grains of plagioclase (oligoclase to andesine composition) with anhedral rounded or polygonal shapes in section. Up to 5% of the rock is composed of garnet, represented by small round to elongate poikiloblasts. Minor quartz (typically 5%) is also present, and traces of sphene and biotite are common.

2.3. Meta-diorite, -tonalite, -granodiorite and -trondhjemite

These lithologies occupy the cores of the dome structures in the WHC. The most common is meta-tonalite, though the core of dome C is occupied by a meta-trondhjemite mass (Fig. 1). Meta-tonalite also forms thick bands within meta-gabbro, especially near the margins of the domes. Rare intact intrusive relationships are preserved, indicating that meta-tonalite has intruded meta-gabbro and meta-diorite, and has itself been intruded by more the felsic meta-granodiorite and meta-trondhjemite (Rashwan, 1991; El Ramly et al., 1993). The lithologies of this group show a range of fabrics from strongly to (more typically) weakly gneissic. Pure linear fabrics are also encountered. Gneissosity is weaker in the lighter-coloured quartz-richer phases mainly for the want of mafic minerals rather than real strain differences. Grain-size is generally coarse (0.8–1.6 mm). The lithologies are distinguished from meta-gabbro by higher amounts of quartz (20–50%) and lower hornblende content (<1%). Minor biotite, microcline,

garnet and sphene are also commonly present, with garnet porphyroblasts contributing about 1%. The main opaque phase is magnetite. The meta-trondhjemites have almost no mafic phases except trace amounts of biotite and chlorite.

2.4. Pegmatites and other minor felsic intrusives

These form usually small masses, or more commonly dykes, which crosscut the gneissosity and are folded and deformed (Fig. 3A). Apart from pegmatite, there are numerous aplite and other microgranite veinlets and dykes. A favoured site for these minor intrusives is shear zones. These dyke phases are particularly common in domes B and C.

2.5. Quartz-rich paragneiss, migmatite and meta-granite

These are fine-grained feldspathic meta-quartzite, micaceous meta-quartzite and quartz-rich gneisses, showing little evidence for preservation of sedimentary structures and textures. Apart from quartz, microcline and plagioclase they contain minor biotite, garnet and sillimanite. Biotite and sillimanite define a weak gneissic banding in these rocks. Locally, the gneissic rocks pass into migmatite with well-developed banding of granitic and pegmatitic leucosomes. Meta-granite is a minor lithology in the studied area. It is also faintly gneissic, with banding mainly defined by biotite.

3. Mesoscopic structures

The mesoscopic structures of the WHC and their map and statistical orientations are described below. We have chosen at this stage not to apply structural terminology (S0, S1, L1, F1, etc.) to these structures (cf. El Ramly et al., 1984). The reasons for this departure are that (a) we regard this contribution as preliminary work, since it is the first detailed structural mapping of this large portion of the WHC, (b) descriptive terms like ''intrafolial fold'' or ''post-gneissosity fold'' are adequate at this stage, and (c) some elements, such as the two generations of post-gneissosity folds, are difficult to distinguish as explained below. In the discussion we will correlate our structures with those listed in El Ramly et al. (1984) and Greiling et al. (1984).

3.1. Gneissic banding

The meta-tonalite and meta-diorite, particularly, show well-developed millimetre-spaced gneissic banding. This banding is parallel to lithological contacts on all scales. The banding is most distinct on the centimetre- and decimetre-scales, where it is clear that the gneissosity is defined by discontinuous planes and wispy surfaces of mafic grain aggregates, and spaced individual mafic grains representing gneissic bands of individual grain thickness. On the scale of a thin section these subtle distributions of mafic grains are not obvious. The mafic minerals are high-temperature metamorphic phases such as decussate to granoblastic hornblende grains and flakes of biotite, the latter with preferred orientation of (001) planes parallel to the gneissosity. Quartz grains are typically elongate parallel to the gneissic foliation. Meta-gabbros may also show gneissosity but are usually simply foliated or have isotropic fabrics. The preferred orientation of the long axes of hornblende grains is best developed in the foliated meta-gabbros.

All gneissic lithologies may also show distinct centimetre- to decimetre-thick lithological banding parallel to the gneissosity (Fig. 2A). This banding often dominates the outcrop, and parallels the gneissosity, but is probably related to stretching out of mixed igneous lithologies (e.g. xenoliths, enclaves, mafic and felsic dykes, sills, etc.) by intense strain, rather than by metamorphic processes. There are occasional rootless intrafolial folds (Fig. 2B), and

Fig. 2. A: Well developed parallel planar banding and gneissosity in meta-tonalite (Dome E). B: Isoclinal rootless intrafolial fold with lower limb sheared out, in gneissic meta-diorite (southeast of Dome C). C: Pressure shadows developed around garnet porphyroblasts in meta-tonalite (Dome C). D: Mineral lineation defined by hornblende rich streaks, in foliated amphibolite (Dome E). E: Continuous planar foliation surface in meta-tonalite, showing extension lineations with curvilinear geometry (lineations pitching to the left in the left half of the photograph and curving to subhorizontal in the right half) (southeast of Dome C). F: Large boudin of meta-gabbro with injections of pegmatite disrupting the boudin neck (south of Dome C). G: Linear tectonite fabric defined by alignment of hornblende grains in meta-gabbro (southeast of Dome C).

low-angle discordances between planes of gneissosity. The latter are probably shear truncations as discussed later.

The regional orientation pattern of gneissosity is shown in Fig. 4B. A stereogram of the orientation for the total gneissosity data for the WHC is shown on

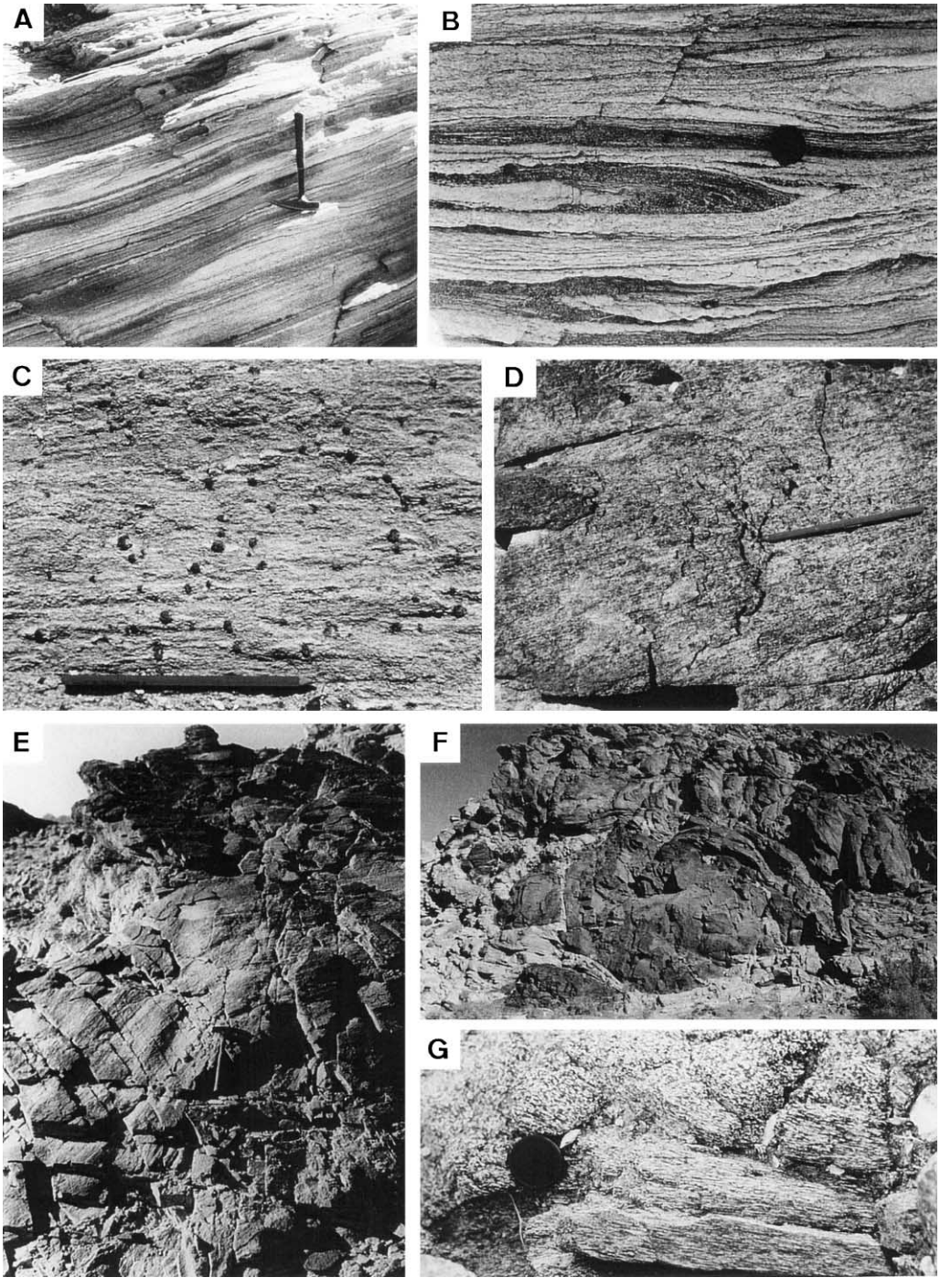

Fig. 5, where we see that moderate S to SW dips are predominant, and NW-trending sub-vertical attitudes are also well-represented.

3.2. Mineral lineations and linear fabrics

On the majority of the gneissosity surfaces are faint to strongly developed mineral lineations defined by linear aggregates of hornblende or biotite grains with preferred orientation of individual mafic grain long axes parallel to the lineation (Fig. 2D). These lineations show smoothly varying patterns of orientation throughout the WHC (Fig. 4A). They are parallel to pressure shadow lineations (Fig. 2C) and stretched pebble and breccia clast long axes in the metasediments (El Ramly et al., 1984; Greiling et al., 1988), and are therefore considered to be extension lineations, parallel to the X direction of the strain ellipsoid. Locally, the lineation may dominate the fabric of the rock so that gneissosity disappears and a linear fabric takes its place (Fig. 2G). There is no change in lineation orientations from zones of gneissic fabric to zones of linear fabric, and there is no special association of the linear fabrics with any lithology.

Abdel Khalek and Abdel Wahed (1983) have noted that there are many instances of more than one mineral lineation on gneissosity surfaces in the northern parts of the W1HC. We have found examples of curvilinear mineral lineations on single gneissic surfaces (Fig. 2E), and examples where the lineation pitches differently in the gneissic bands one above the other, but no examples of more than one lineation on a single gneissosity surface. Greiling et al. (1988) reported variable extension lineation trends, including NE–SW- and NW–SE-trending lineations, which they believed to be due to different tectonic transport directions. We find that these trend variations are all part of a continuum, defining curvilinear trajectories as seen in Fig. 4A. The extension lineations for the entire WHC area (Fig. 5) show gentle to moderate plunges to the SE, SW and NW. The significance of these patterns is discussed later.

3.3. Intrafolial folds

There are numerous tight to isoclinal folds, with axial planes approximately parallel to the plane of the gneissosity, and hinges lying at a small angle to the local extension lineations (Figs. 3A,B, 4A and 5). These folds are developed in felsic bands and pegmatite dykelets (especially in domes B and C), and folded mafic bands (which may represent extremely strained enclaves, etc.). Where fold limbs are thinned out, these folds form rootless intrafolial fold hooks (Fig. 2B). The folds may be symmetrical, but are usually asymmetrical. The S- and Z-asymmetry does not apparently define clear vergence domains (Fig. 6).

3.4. Boudins and pinch-and-swell structures

Boudins and pinch-and-swell structures are developed on all scales (Fig. 2F) up to kilometre-long boudins in massive meta-gabbro layers, e.g. those along the eastern and southeastern margins of dome C (Fig. 4A,B). Boudins commonly form by extension of the limbs of the tight to isoclinal intrafolial folds. Where they are completely exposed, the boudins are always seen to be elliptical to rhombic shape in the plane of the gneissosity, and lens-shaped in planes normal to the gneissosity. They are therefore chocolate-tablet boudins rather than sausage-shaped boudins. The boudins are commonly widely separated, indicating that the gneissosity is a plane of considerable flattening and extension.

3.5. Mylonite zones

Thin mylonitic shear zones are most commonly found within massive meta-gabbro, where they show excellent shear sense indicators in the form of curved shear foliation trajectories in the shear zone walls

Fig. 3. A: Isoclinal intrafolial folded felsic veinlets in foliated meta-trondhjemite (Dome C). B: Tight asymmetric folded veinlets in foliated meta-diorite with axial planes parallel to the foliation (southwest of Dome C). C: Rounded post-gneissosity folds in gneissic meta-tonalite (Dome D). D: Complex style of post-gneissosity folds in interlayered amphibolite and gneissic meta-tonalite (eastern margin of Dome D). E: Post-gneissosity folds with almost recumbent attitude (between Domes B and C). F: Ductile shear zone with dextral strike-slip shear sense in gneissic meta-diorite (southeast of Dome C). G: Isotropic fabric in meta-gabbro passing into ductile shear foliation (southeast of Dome C). Sense of shear is hangingwall (upper part of photograph) moved northwest relative to the footwall.

(Fig. 3G). The mylonites now have variable orientations but are generally parallel to the nearby gneissosity orientations. They were therefore probably of the same original orientation as the gneissosity. Mylonitic lineations however are more variable in their orientation. It is difficult in each case to

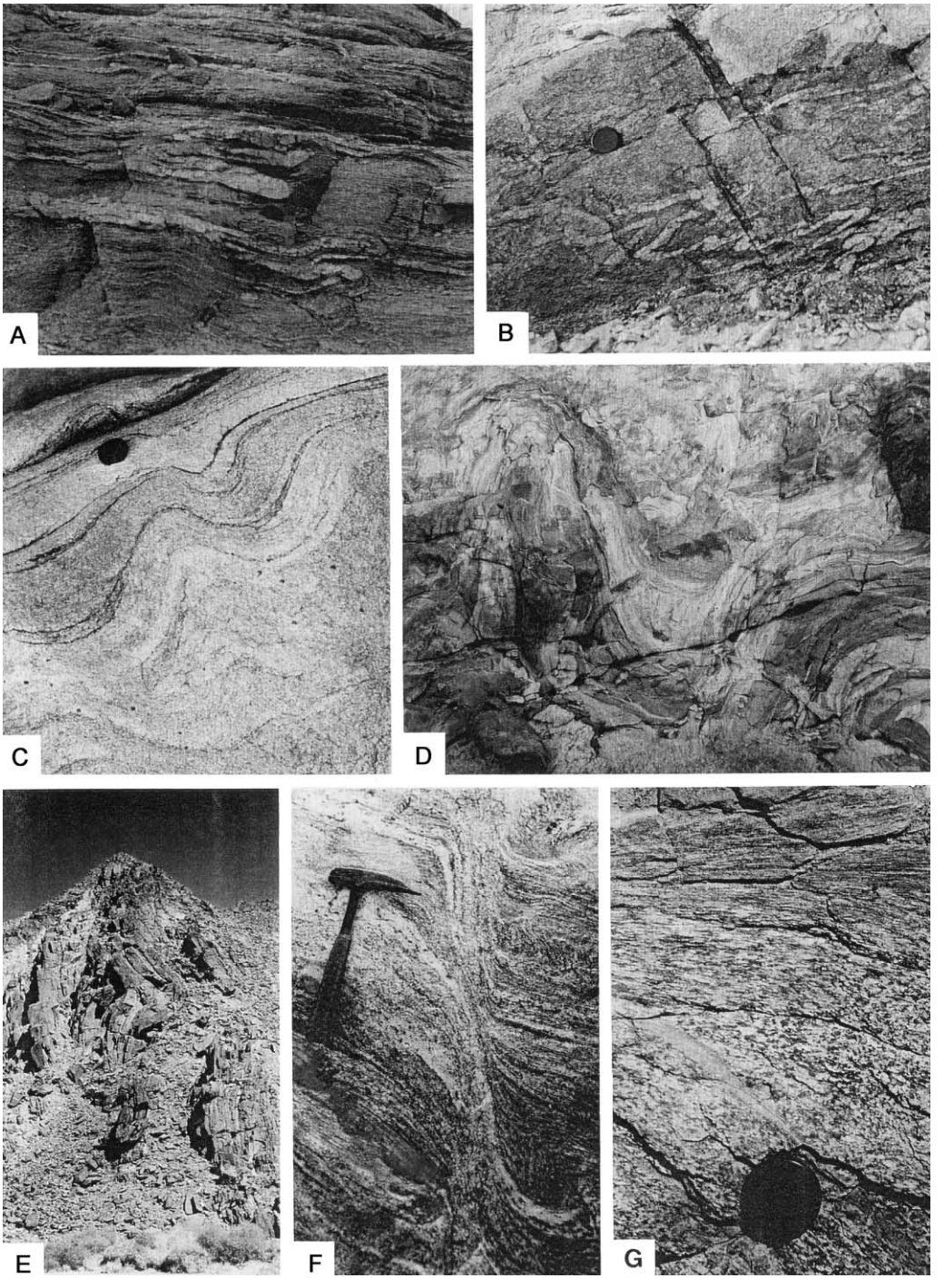

know the timing of the formation of the mylonite zone. Those with foliations defined by high-temperature metamorphic minerals of the same assemblage as the enclosing gneisses, and which show tight folding about axial planes parallel to the gneissosity are probably of similar age to the gneissosity.

3.6. Post-gneissosity folds

Open to tight folds with axial planes approximately at right angles to the gneissosity are amongst the commonest structures in outcrops (Fig. 3C,D). Over large areas of the WHC, these folds have usually steep axial planes, and hinges dipping towards all quadrants (Figs. 4B and 5). These post-gneissosity folds do not possess an axial plane structure, unless they are tight, in which case the axial plane structure is a weak foliation described by flattened grains. This foliation is not evident in areas away from the zone of tight folding. The mesoscopic post-gneissosity folds commonly have wavelengths of decimetres to tens of metres. In many outcrops, especially in the southeastern half of Dome D, it is evident that there are two sets of such folds with axial planes at right angles to each other, one generally trending NE–SW or ENE–WSW, and the other trending NW–SE or NNW–SSE (Figs. 4B and 5). A problem in the interpretation and recording of these folds is that the two generations show no obvious differences in style, and their interference on the mesoscopic scale is type 1 (dome-and-basin), which does not allow relative age determination. They clearly exist as two groups, but to attach terminology to them in the field is difficult. We have grouped all of these folds into one category for the purpose of statistics and map orientation, but we expect that future study will provide a criterion for better distinguishing the two generations in outcrop.

3.7. Extensional and transcurrent ductile shear zones

An interesting set of structures in the WHC includes extensional and transcurrent ductile shears. These cut across all of the above structures, hence, are late-stage structures. Some shear zones are of limited extent (Fig. 3F), while others form extensive low-dipping sheets showing only slight folding effects. The former are often invaded by pegmatitic fluids, the latter by felsic dykes that have become mylonitized.

4. Macroscopic structural analysis

4.1. Peculiarities of the macroscopic fold structures of the WHC

For convenience, we have continued to refer to structures A to E in the WHC as "domes". Ghosh (1993, p. 224) defines a dome as "an antiformal structure with no distinct trend of the hinge line". Most of the Hafafit granitoid gneiss-core structures fit this definition, though structure D has margins close to vertical along most of its perimeter, and elsewhere the margins dip towards or away from the centre of the structure, so that it is unclear from some cross sections whether it is antiformal or synformal.

The shape, size and orientation of domes A to E are variable. Dome A shows a classic elliptical shape with NW-trending long axis, while dome E is more elongate and teardrop-shaped, with long axis trending WNW. Dome C is elliptical to rectangular with long axis trending NE. Dome B has the appearance of a crescentic dome (of possible type-2 fold interference origin), with a flexure in its NE end, but is generally elongate in a NE direction. Dome D is the largest structure and has a rectangular to elliptical shape, with approximately NW-trending long axis, and a dramatically narrower northwestern extension. Apart from size, shape and orientation variations, the WHC structures show other peculiarities as interference structures, namely:

(1) While domes are well developed, no basinal structures are evident and synformal structures of any kind are subdued. Likewise, saddles are not evident in this interference pattern.

Fig. 4. A: Map of a portion of the WHC from NW of dome D and including domes B, C, D and E, showing the orientation of intrafolial fold hinges (drumstick symbol) and extension lineations (arrows). B: Same area as for A, showing the orientations of gneissic layering (dip-and-strike symbol) and post-gneissosity fold hinges (arrows). Areas of coarse stipple are dominantly meta-psammitic rocks and migmatites. Finely stippled areas represent meta-gabbros, foliated amphibolites and meta-diorites. Areas of meta-tonalite are shown without ornament. A–A′, B–B′–B″–B‴, C–C′, D–D′ are cross-section lines. C: Interpreted vertical cross-sections from section lines shown in B.

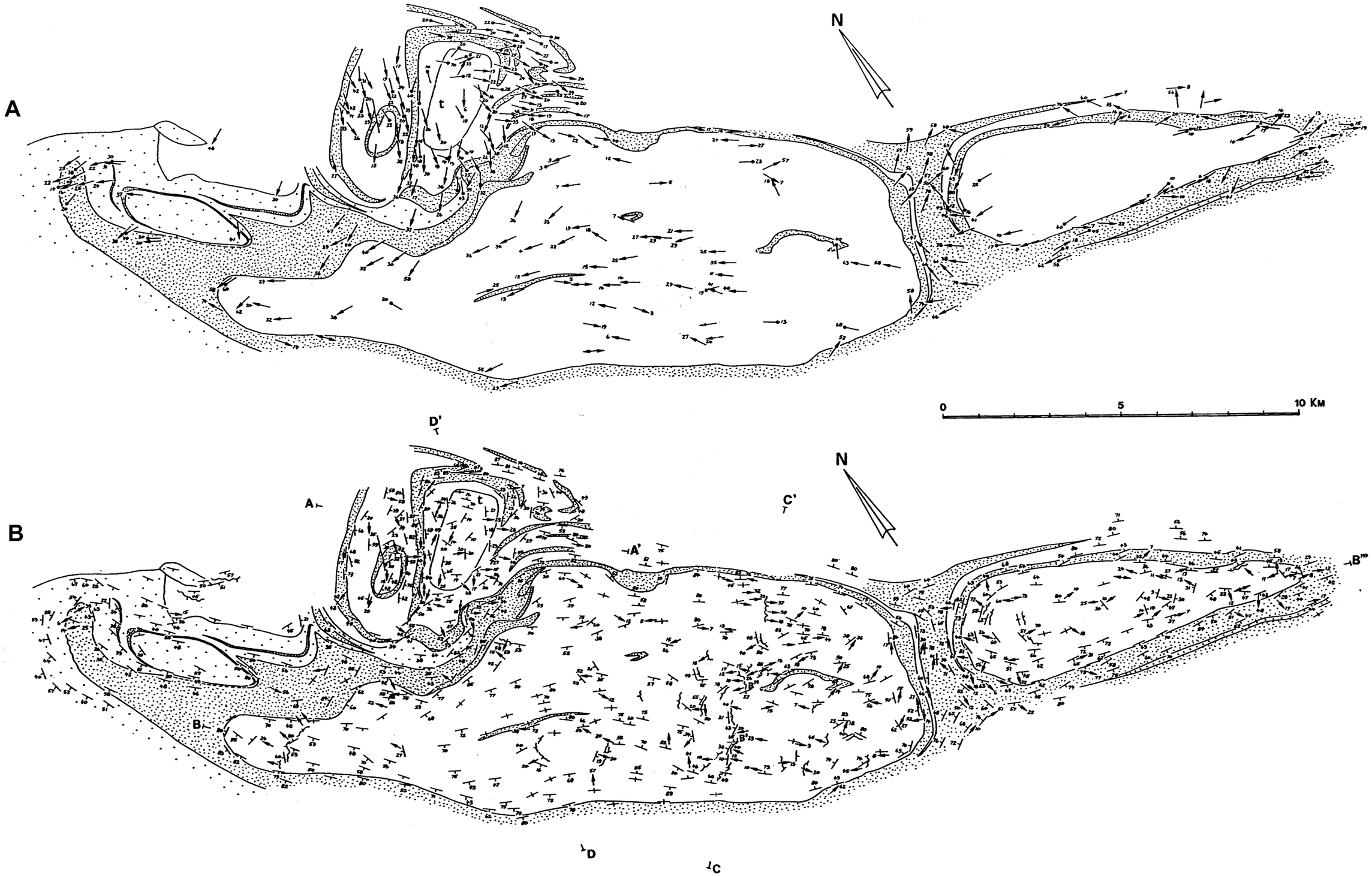
A
N
t
0
5
10 Km
B
D'
A
C'
A'
B'''
B
B'
D
C

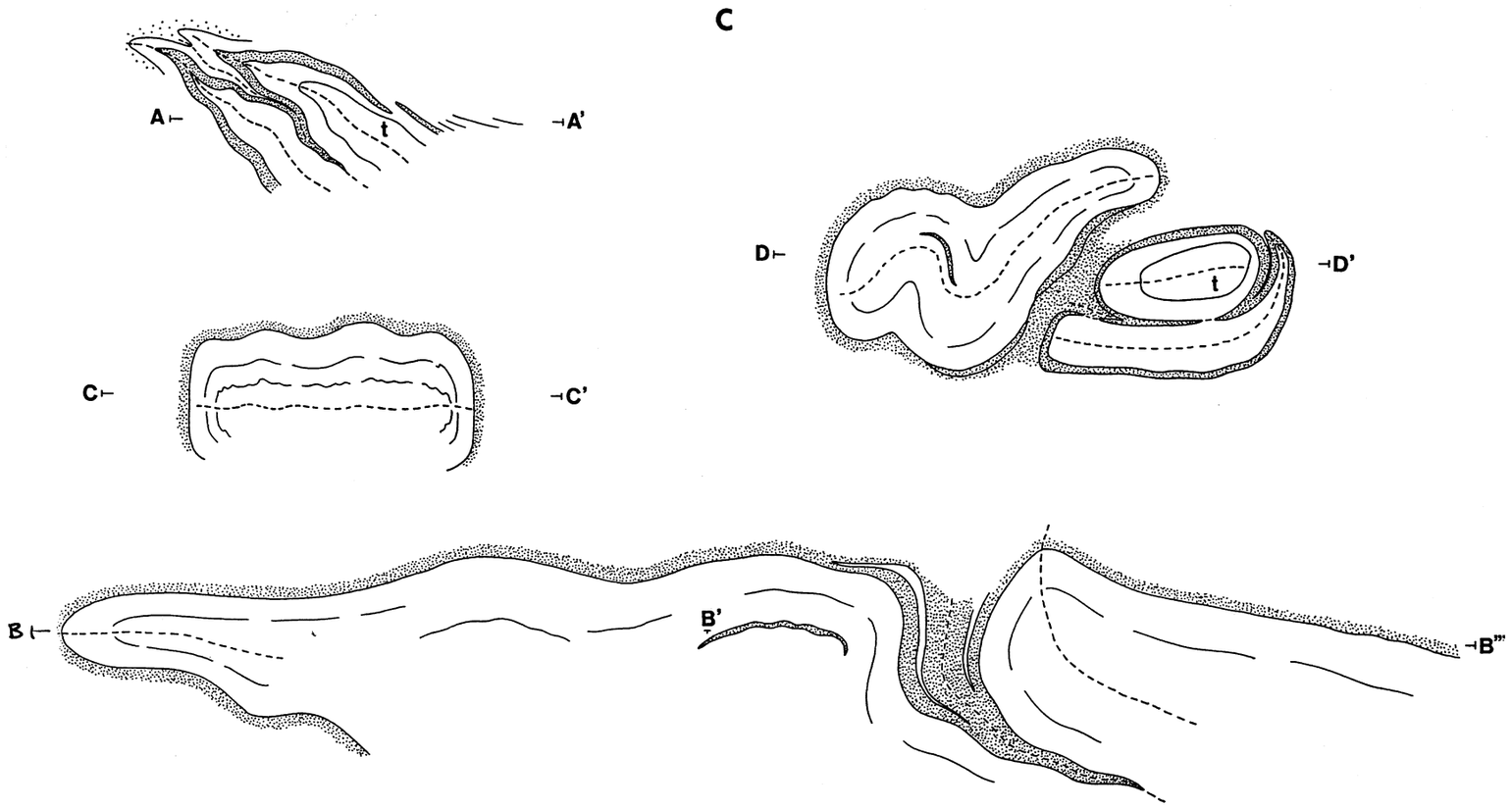

Fig. 4 (*continued*).

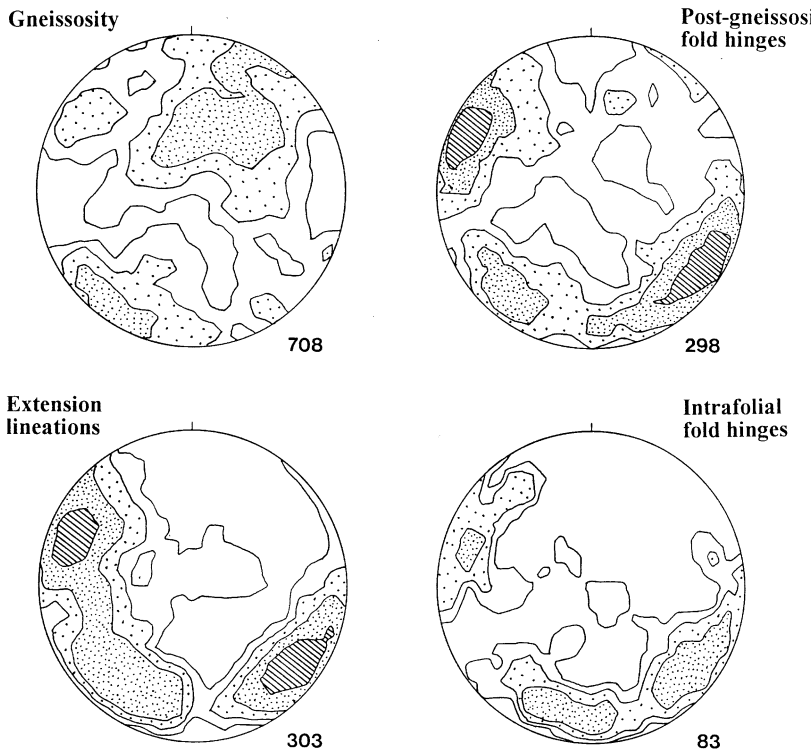

Fig. 5. Density-contoured lower hemisphere Schmidt net stereograms of structural data from the WHC. Shading symbols for all stereograms are from highest to lowest concentration: diagonal striping, fine stippling, coarse stippling, no ornament. "Gneissosity" stereogram represents poles to 708 gneissosity measurements for the entire area of study. Contours are 1%, 2% and 4%. "Extension lineations" stereogram represents 303 mineral lineation measurements for the entire area of study. Contours are 1%, 2%, 4% and 8%. "Post-gneissosity fold hinges" stereogram represents 298 post-gneissosity fold hinge measurements for the entire area of study. Contours are 1%, 2%, 4% and 8%. "Intrafolial fold hinges" stereogram represents 83 intrafolial fold hinge measurements for the entire area of study. Contours are 2%, 4% and 8%.

(2) The domes are concentrated in a narrow NW–NNW-trending zone, rather than forming a uniformly distributed set of structures, side by side.

(3) Axial traces of the domes, interpreted from the map, are generally discontinuous with only a few continuing from one dome to the next. One exception is the fold along Wadi Abu Higilig (see Fig. 1 for location) between domes B and C; and domes D and E have been previously interpreted to share a common NW–WNW-trending antiformal element. Other extrapolations of axial traces between domes have been illustrated by Greiling and El Ramly (1990), but have little supporting evidence (see later discussion).

These above features (points 1 to 3) are not usual for dome-and-basin interference patterns (either fold interference types 1 or 2). A possible explanation for this is that at least one of the fold generations is unusual in style. In the next section we present evidence that the first generation of macroscopic folds in the WHC is unusual in having sheath fold geometry.

4.2. Reasons for considering sheath folds

Some properties of sheath folds, which explain the above peculiarities of the WHC domal interference pattern and outcrop features, are as follows:

1. When sheath folds form within gently dipping tabular shear zones, the synformal elements of the sheaths are usually difficult to recognize since they may be sheared out systematically along low-dipping ductile shears or are strongly flattened.
2. Sheath folds need not show any special spatial relationship one to another (i.e. they are not necessarily developed side by side or with

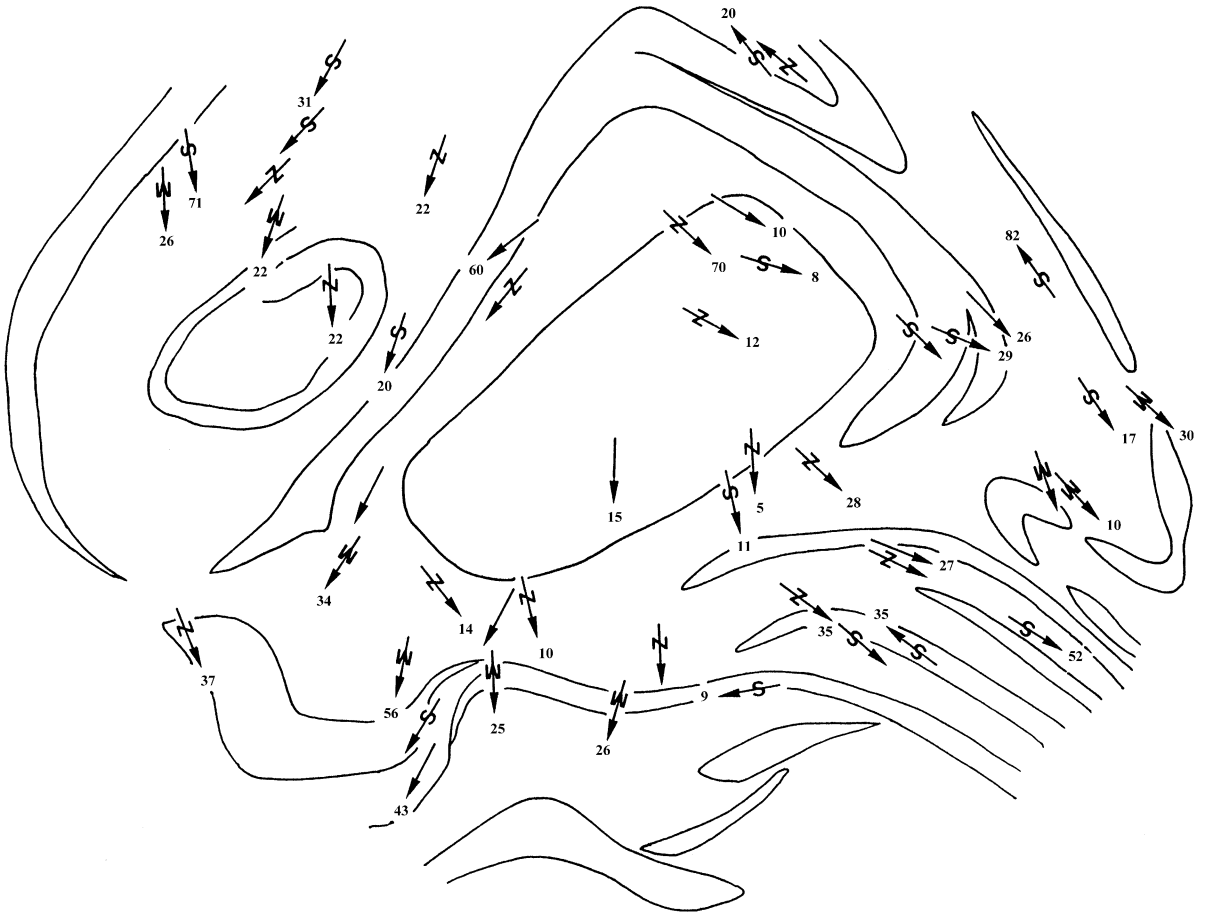

Fig. 6. Map of the area including domes B and C, showing the distribution of intrafolial fold S-, Z- and M-symmetries.

some regular wavelength), however, they show elongation in the same direction, the direction of regional extension.

3. Sheath fold axial planes are usually not continuous. One of the reasons for this is that sheath folds often form from pimple-like perturbations in layering, or from folds with initially short axial lengths.
4. Sheath folds are characteristic of zones of strong extensional strain, especially regimes in which the extension is associated with sub-horizontal ductile shear zones. They are therefore commonly associated with intense extension lineations and linear fabrics.
5. Sheath folds have strongly curvilinear hinges with parasitic folds on their limbs rotated to near parallelism with stretching lineations.

Macroscopic sheath folds have been reported by Rhodes and Gayer (1977), Williams and Chapman (1979), Henderson (1981), Lacassin and Mattauer (1985), Vollmer (1988) and Goscombe (1991). We present the evidence below for the existence of macroscopic sheath folds in the WHC. However, it should be noted that no sheath folds of mesoscopic scale have so far been discovered in the WHC. The intrafolial folds do not show sheath geometry, and there are ample opportunities to see these folds in any section. They appear to be essentially cylindrical in form. The existence of mesoscopic sheath folds is not a pre-requisite for the identification of macroscopic sheath fold geometry. Henderson (1981) and Lacassin and Mattauer (1985) noted similar deficiency of mesoscopic sheaths on the limbs of macroscopic sheaths. A possible explana-

tion for this comes from Cobbold and Quinquis (1980), who noted that, for the same strongly extensional strain history, folded layers whose mechanical behaviour is passive are more sheath-like in form than those which have a mechanically active behaviour. The smaller scale folds at the WHC are defined by dyke lithologies within the gneisses, and these may have a more mechanically active behaviour during fold amplification than the macroscopic folds, which are in meta-tonalite outlined by foliated meta-gabbro.

Before investigating the role of sheath folds in the macroscopic analysis of the WHC structures, and exploring their subsequent deformation, it is worthwhile clarifying some of the terms used to describe sheath folds.

4.3. Sheath fold terminology (Fig. 7)

Sheath folds are plane noncylindrical folds with strongly curved hinges. They have an axial plane, and may therefore be described as upright, inclined or horizontal. The strongly curved hinge negates the use of terms like horizontal or plunging, which describe the orientation of the fold hinge. It is preferable to describe the attitude of the sheath in its axial plane via the sheath fold cone axis (Fig. 7A). Thus, the cone axis may be horizontal, plunging, vertical, etc. The cone axis may also be considered as a vector that points in the direction in which the sheath is convex. If this vector points upward the sheath is antiformal; if downward, synformal, otherwise it is neutral.

The angle between tangents to the hinge (in the axial plane), measured across the cone axis is called the hinge line angle (ω) (Fig. 7A) (Williams and Chapman, 1979). The angle between the limbs measured in the plane along the cone axis and at right angles to the axial plane is called the interlimb angle (α) (Fig. 7B). For true sheath folds the ω angle should lie between 20° and 90°. Unfortunately, the ω angle is extremely difficult to measure in macroscopic sheaths.

Sheath folds are usually elliptical in sections perpendicular to the cone axis (also called the *x*-axis). In such sections, the long axis of the ellipse is referred to as *y*, and the short axis is called *z* (Skjernaa, 1989).

4.4. Extension lineation patterns on sheath folds

It is important here to very briefly consider the pattern of extension lineations on sheath folded surfaces, since these lineations will be used to locate sheath folds in the WHC. This topic has not been treated directly in the literature but can be inferred from models for sheath fold development. The precise strain distribution on the surface of the sheath fold will of course depend on the final shape of the sheath fold and the shape of the initial perturbation, which gave rise to it. If the cross section of the sheath fold is circular (i.e. the sheath is a regular cone), then the extension lineations will be rectilinear and will be disposed along the cone surface generators (Fig. 7C). The tip of the conical fold will experience equal extension in all radial directions so no extension lineation will exist at the tip.

In the more general case where the sheath fold has an elliptical cross section, the likely patterns of extension lineations are as shown in Fig. 7D. In this series of sketches, flattening and axial extension of the conical fold produces more elliptical cross sections, gradually modifying the radial pattern of lineations on the circular cone. In the process, the radial lineations migrate towards the sheath fold hinge and acquire curvature especially near the tip of the sheath fold. This is due to the noncoaxial strain history on most parts of the sheath fold surface. Lineations in the *xz* plane will not rotate out of that plane. The result is that one may expect curved lineations on sheath fold limbs, with obtuse angles between the trends of these lineations. This angle depends not only on the bulk strain but varies also with distance from the sheath fold tip. This angle therefore has limited value in estimating the ω angle, even in the absence of later deformations. The extension lineations will be expected to fade towards the tip of the fold but may be present at the tip since the extension there will not be equal in all directions.

4.5. The sheath folds of domes B and C, and their refolding

The area consisting of domes B and C provides the clearest indication of the presence of macroscopic sheath folds in the WHC. The trends of extension lineations and sub-parallel intrafolial fold hinges

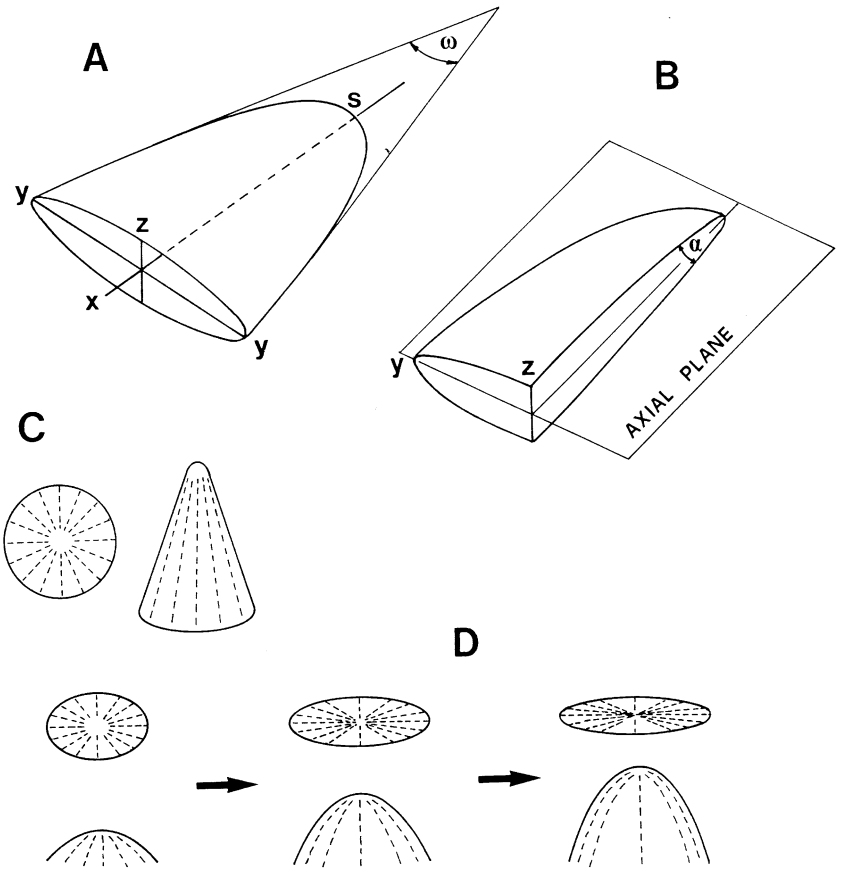

Fig. 7. A: Idealized sketch of a sheath fold showing element ω (hinge angle) and axes x, y and z. The x-axis is the cone axis of the sheath. The sheath hinge lies along the line curving from y to s to y. B: Idealized sketch of a sheath fold cut along the xz plane to show the element α (interlimb angle) and the axial plane (the xy plane). C: Radiating pattern of extension lineations on the surface of a circular conical fold, for the case where the conical fold has amplified by coaxial extension along the cone axis. D: Proposed pattern of extension lineations on the surface of a sheath fold which has amplified (as shown by figures from left to right) by coaxial extension along the cone axis, with simultaneous flattening normal to the sheath fold axial plane.

(Figs. 4A, 6 and 8) describe arcuate trajectories in that area, with lineations gradually changing from SE-ward plunges, in the east, through E–W trends, to SSW-ward plunges in the western part of the area. At first sight, these arcuate lineation and fold hinge trajectories appear to be a result of folding about a north–south-trending axial plane along Wadi Abu Higilig (see Fig. 1 for location, and Fig. 4A), since the change in lineation trend is approximately symmetrical about the axial plane of this fold. However, it is easy to demonstrate that unfolding this fold will not restore the lineations to a common lineation orientation. Fig. 9A represents the average orientation of the lineations on the limbs of this fold. On the fold's western limb (defined by a NE-striking steeply dipping strip of meta-gabbro) the lineations subtend an angle of about 60° with the steeply plunging fold hinge (between the fold hinge and lineations "m" on Fig. 9B). The same lineations on the vertical SE-trending eastern limb subtend an angle of about 120° with the hinge (measured as shown in Fig. 9B for lineations "n"). After unfolding (Fig. 9B,C) a pitch angle difference of about 120° between m and n is retained. It is clear from this that the deflected lineation trends, represented by m and n, existed *before* the fold along Wadi Abu Higilig. The diver-

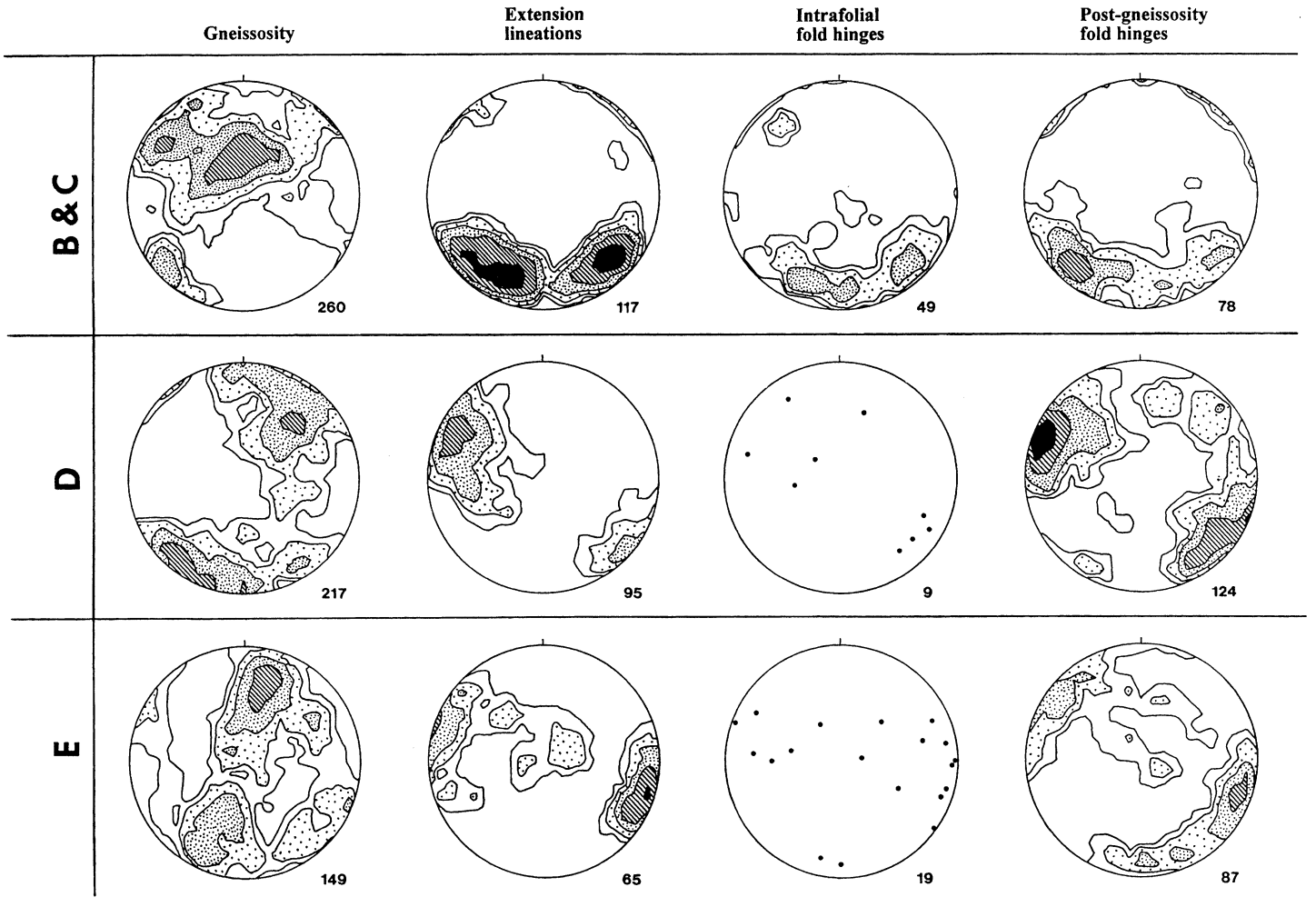

Fig. 8. Density-contoured lower hemisphere Schmidt net stereograms of mesoscopic structural elements from the WHC, separated into data from domes B and C, D and E. Shading symbols for all stereograms are from highest to lowest concentration: black, diagonal striping, fine stippling, coarse stippling, no ornament. "Gneissosity" stereograms: B and C (260 poles, contours 1%, 2%, 4% and 8%); D (217 poles, contours 1%, 2%, 4% and 8%); E (149 poles, contours 1%, 2%, 4% and 8%). "Extension lineations" stereograms: B and C (117 measurements, contours 1%, 2%, 4%, 8% and 16%); D (95 measurements, contours 2%, 4%, 8% and 16%); E (65 measurements, contours 2%, 4%, 8%, 16% and 32%). "Intrafolial fold hinges" stereograms: B and C (49-fold hinge measurements, contours 3%, 6% and 12%); D (9-fold hinge measurements); E (19-fold hinge measurements). "Post-gneissosity fold hinges" stereograms: B and C (78-fold hinge measurements, contours 2%, 4%, 8% and 16%); D (124-fold hinge measurements, contours 1%, 2%, 4%, 8% and 16%); E (87-fold hinge measurements, contours 2%, 4%, 8% and 16%).

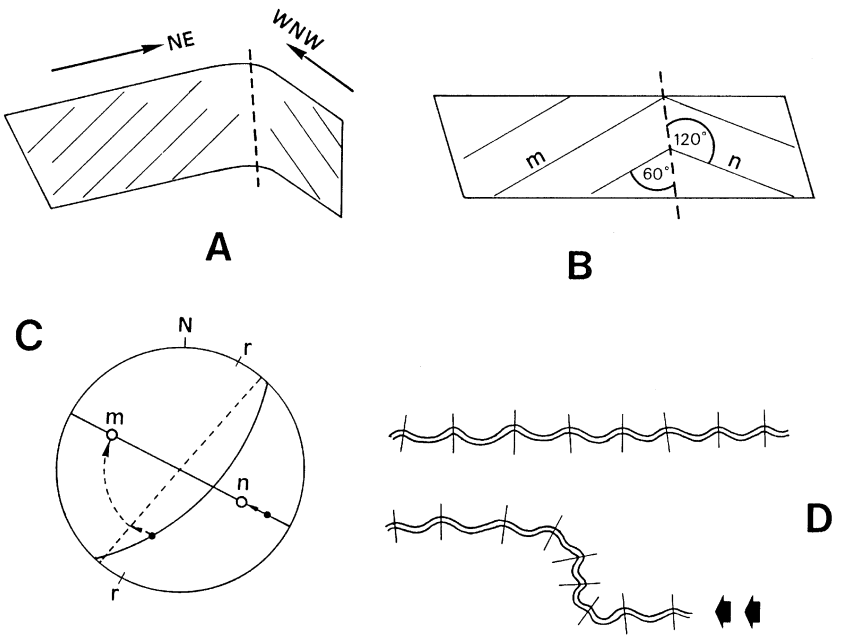

Fig. 9. A: Simplified sketch of the folded sub-vertical monoclinal limb between Domes B and C showing the average orientation of extension lineations on each limb of this fold. B: Unfolding the fold in A, by rotating the limbs to a common orientation for both limbs, does not bring the extension lineations to a common orientation, i.e. the different lineation trends on opposite sides of the fold are not due solely to folding. The lineations on the western limb are represented by the letter "m", while those on the eastern limb are labeled "n". C: Stereographic representation of the unfolding procedure. The two dark great circles represent the NE-and WNW-striking limbs of the fold in A. First, the line of intersection of the two limbs is brought to the vertical by rotating about the pole to the WNW-striking limb (represented by r). This rotation also brings the lineations on the WNW-striking limb to the line n. Unfolding the now-vertical NE-striking limb brings the lineations on it to line m. The approximate angle between the lineations on the two limbs after unfolding is about 120°. D: Sketch showing the origin of the gently reclined to recumbent open folds observed on steeply dipping foliations. These folds have formed by rotation of formerly upright folds, by monoclinal refolding.

gence of the lineation trends continues into the southern part of dome C (Fig. 4A), where the modest changes in the orientation of gneissosity indicate only gentle folding (Fig. 4B). There exists additional evidence for original curved trajectories of extension lineations in this area. At an outcrop near the point where the lineation trends diverge (location "Λ" in Fig. 6), the lineations are clearly curved on a *planar* gneissosity surface (Fig. 2E). Their curved trends are therefore not the result of later folding of originally homogeneous trends, and their original macroscopic curvature is consistent with the large scale folds having significantly curved hinges, as exemplified by sheath folds.

Cross section A–A′ (Fig. 4C) across domes B and C indicates that both B and C are tight to isoclinal antiformal structures with axial planes dipping roughly SE-wards. The antiform associated with dome B is interpreted to be a sheath fold (or at least a strongly noncylindrical plane fold with curved hinge) on the basis of the extension lineations approximately following the trend of its long axis. The continuation of the same lineation pattern into the area of dome C suggests that this dome also incorporates a sheath fold. The strip of meta-gabbro separating domes B and C shows a very sharp re-entrant to the NE of dome C (Figs. 4A and 6). This is an extremely attenuated synformal structure separating the B and C sheath antiforms. This synform does not extend farther west than the western edges of domes B and C, nor can it be traced any farther than the eastern edges of these two domes. The extreme attenuation and limited extent of this synform is normal for sheath folding.

In addition to locating the antiforms associated with domes B and C, the cross section A–A′ reveals that these antiformal structures are themselves folded into monoclinal flexures and open folds. The monoclines are responsible for the alternating domains of gently dipping to sub-vertical gneissosities seen in cross section A–A′ and represented as the concentrations of moderate to steep S, SE and SW-dipping gneissosity poles in Fig. 8. A representation of the shapes of sheath folds of domes B and C, and their later refolding to monoclines is shown in Fig. 10A,B. There are also open upright post-gneissosity folds with dominantly SW-trending hinges, which precede the monoclinal flexing, since the same folds are represented by NE-/SW-trending recumbent to gently inclined folds on the steep limb of the monoclines, apparently having been rotated to these orientations during monoclinal flexuring (Figs. 3E and 9D).

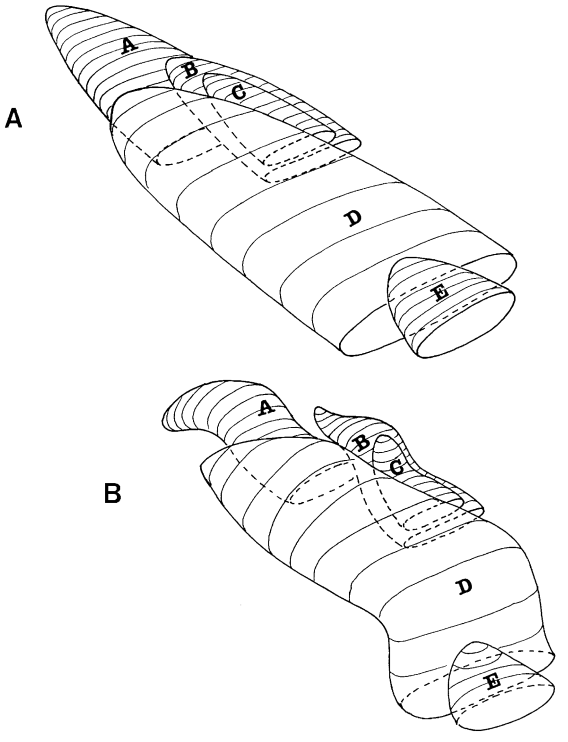

Fig. 10. A: Sketch of the interpreted shape and relative position of the sheath folds forming the first folding in the WHC. Each sheath shown in A corresponds to one of the later interference domes, and are labeled A to E accordingly. B: Later macroscopic flexing of the sheaths in A to form monoclines and other fold structures. See text for discussion.

Before exploring the possibilities of sheath folds in the other domes of the WHC, we will complete an examination of domes B and C to understand how they have attained their present configuration. The most obvious subsequent deformation is the bending of the steep monoclinal limb separating B and C around the N–S-trending fold along Wadi Abu Higilig. This folding is associated with the bending of the eastern end of the sheath fold of dome B around the eastern side of dome C. This final refolding of dome B by E–W/NE–SW shortening is represented in Fig. 11B, which also explains why the fold at the eastern extremity of dome B has a sub-vertical plunge. This latter fold is interpreted to change from steep to gentle plunge at depth as shown in Fig. 11B and on cross section D–D′ (Fig. 4C). The peculiar closed elliptical outcrop in the western half of dome B is interpreted to be a cross section through a small sheath folded layer within the main dome.

Apart from some SE-trending open upright folds in the gneissosity (see Fig. 4B), Dome C does not appear to show clear later refolding effects, except in two areas. These are the northward convex flexure in metasedimentary gneisses and meta-gabbros along the SW margin of dome C, and the almost rectangular shape of this dome at its eastern end. The second effect requires some explanation, which will assist with the interpretation of the other domes of the WHC. We illustrate the deformation of the monoclinally folded sheath fold precursor leading to dome C in Fig. 11C. The principal deformation effect in dome C, produced by the same E–W or NE–SW shortening as has affected dome B, is the change in the aspect ratio (y/z ratio) of the sheath fold. This is an interesting aspect of the deformation of sheath folds, which is later discussed. Greater flattening on the eastern side has produced the rather rectangular end defined by vertical gneissosities. We must be careful to distinguish the sharp flexure in the NE end of dome C, and the flexure in the monoclinal limb separating domes B and C, as separate folds.

The distinct fold pair that affect the meta-gabbro mega-boudins, SE of dome C (Fig. 4A,B), are later folds in the sheath envelope of domes B and C. These folds are not continuations of the bent eastern end of the dome B. The gently arcuate trends of gneissosity

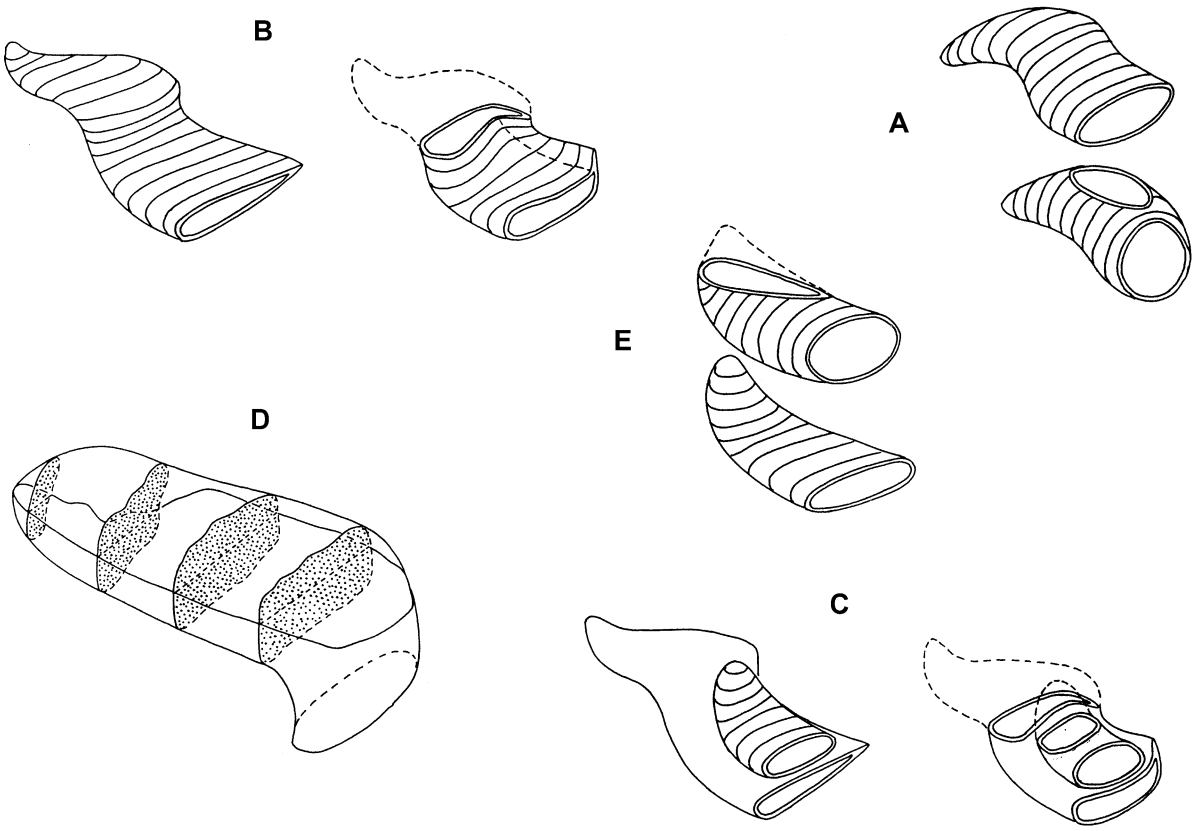

Fig. 11. Diagrams showing the interpreted shapes of the sheath folds before (except D) and after the last macroscopic folding event (related to NE–SW shortening). Each figure relates to the dome of the same alphabetic letter, i.e., Fig. A is relevant to dome A, Fig. B to dome B, Fig. C to dome C, etc. In each figure the outcropping shape of the dome is also shown as a section through the refolded fold. A: top figure before, bottom figure after the latest refolding. B: left figure before, right figure after the latest refolding. C: left figure before, right figure after the latest refolding. Both domes B and C are shown in this figure. D: 3D sketch of the sheath for dome D showing several cross sectional shapes. E: bottom figure before, top figure after the latest refolding.

around the SE end of dome C prohibit the connection of the axial plane of the fold pair with the fold at the eastern end of dome B.

4.6. The sheath fold of dome E, and its refolding

Dome E has a teardrop shape with consistently outward dipping gneissosity at its margins (Fig. 4B). The gneissosity at its NW end dips radially outwards at 40–80°. The dips decline gradually along the dome margins towards the SE tip of the dome, where the gneissosity dips about 15° to the southeast. The stereogram of poles to gneissosity from dome E is presented in Fig. 8. The poles to gneissosity from the NW half of the dome describe a small circle on the stereogram in Fig. 12A, and therefore show that this NW end has a conical geometry with near vertical cone axis. The gneissosity data from the SE half of the dome demonstrate cylindrical geometry (Fig. 12B) with gently SE-plunging fold axis. The gneissosity rapidly attains very steep to sub-vertical attitudes away from the margin of the dome, on its NNE and SSW flanks. Gneissosity orientations between domes E and D are rather complex (Fig. 4B). The expected synformal structure between the two domes is not obvious, as gneissosities pass from N to NW dips through vertical, to S or SE dips. Domes D and E are bounded north and south by almost straight gneissosity trends showing no clear signs of a synform extending NE or SW beyond the width of domes D and E.

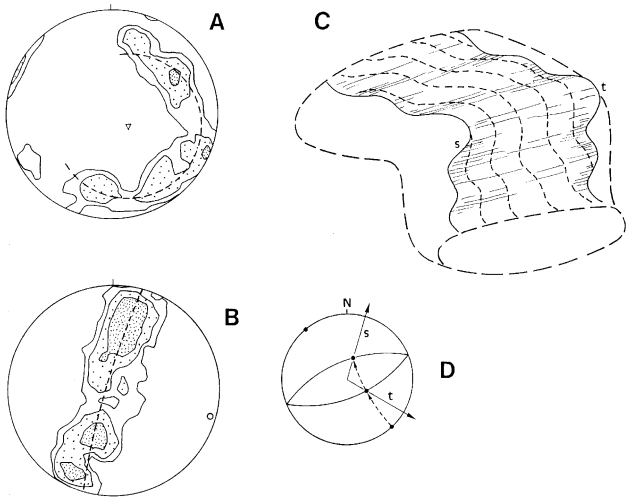

Fig. 12. A and B: Density-contoured lower hemisphere Schmidt net stereogram for poles to gneissosity from dome E. A: represents the NW one-third of the dome, and shows a small circle pattern of poles. B: represents the SE two-thirds of the dome, and shows a great circle pattern of poles. See text for discussion of the significance. C: figure representing a portion of the SE end of dome D showing how the gneissosity along this SE end of the dome changes dip from moderate inwards towards the dome (at s, representing the S tip of the dome) through vertical to steep outwards from the dome (at t, representing the E tip of the dome). These dip changes are due to slightly oblique monoclinal refolding of an earlier upright macroscopic fold. Extension lineation trends are also shown as dotted lines. D: Stereographic projection figure showing originally NW-trending horizontal lineations, which have become rotated along with the gneissosity during monoclinal folding to produce steeply NNE plunging lineations at s and steep SE-plunging lineations at t.

The above gneissosity patterns may be explained if dome E is an antiformal sheath fold modified by folding and flattening. The absence of a well developed synformal structure between D and E is similar to the situation for domes B and C. The conical end of dome E is easiest to explain as a flattening modification of the already conical geometry of the tip of a sheath fold (Fig. 11E). The steepness of the cone axis is due to bending back of the sheath fold against the monoclinal flexure, which defines the SE end of dome D, as shown in Fig. 11D and on cross section B″–B‴ (Fig. 4C). The flattening modification of the steepened conical sheath tip has also caused the low curvature upper limb of the sheath to fold cylindrically (Fig. 11E). This figure also demonstrates why the dips of gneissosity gradually decline towards the SE tip of the dome, and why gneissosity dips steepen rapidly away from the dome margin. It also explains the tear drop shape of dome E.

Extension lineation patterns confirm a sheath fold model for this dome. At the NW circular end of the dome, these lineations plunge steeply outwards, and are interpreted to lie on the upturned lower limb of the sheath (Fig. 4A). Elsewhere, these lineations have dominantly gently WNW–ESE trends along the dome margins (Fig. 4A). The lineations at the NW end of the dome show rapid changes in orientation to adopt N-plunging attitudes. These trends merge with those of the lineations south of dome D. The reasons for the peculiar lineation trends and gneissosity dips in the area between domes D and E will now be explained.

West of dome E, the extension lineations plunge steeply N towards dome D, and gneissosities dip towards this dome moderately steeply. The extension lineation trends change to steep ENE plunges north of dome E, where the gneissosity dips away from dome D. For the gneissosities between domes D and E, the steepening through vertical is interpreted in the same manner as for the area between domes B and C. In cross section B″–B‴ and Fig. 12C, these patterns are seen to be due to a monoclinal flexure affecting sheaths D and E, which were previously folded into rounded NE-/SW-trending flexures. Post-gneissosity folds with the appropriate orientation are found in this area between D and E (Fig. 4B). As with the area of steep gneissosity between domes B and C, the meso-

scopic NE-trending open folds between domes D and E have gently inclined axial planes due to their rotation from formerly upright attitudes during monoclinal folding. The result of the combination of NE-trending upright flexures and later monoclinal folding is the local overturning of the southern corner of dome D, and gneissosities beyond it, but not those at the eastern corner. Fig. 12C,D shows how the extension lineations beyond the southern corner of dome D are rotated from the usual NW/SE trends to steep northerly plunges, while those beyond the eastern corner adopt the more easterly trends.

The NW-/SE-trending post-gneissosity folds have gentle plunges (Fig. 8). These folds are generally upright and are weakly developed in dome E.

4.7. The sheath fold of dome D, and its refolding

D is the largest dome structure in the WHC. It extends in a NW direction for nearly 20 km. The SE half is uniformly 6–7-km wide while the NW half shows folding of its northern margin as the dome thins to 1.5-km wide. The general NW trend and steep sides of the dome are reflected in the stereogram of poles to gneissosity (Fig. 8). Within the SE half of dome D, the gneissosity traces out kilometre-scale elliptical domes and basins with moderately dipping limbs and a flat-lying upper enveloping surface (cross section C–C′ of Figs. 4C and 14), produced by the type-1 interference of NE-/SW-trending and NW-/SE-trending post-gneissosity folds. The stereogram of gneissosity in Fig. 8 suggests that the NW-/SE-trending folds are the tighter, in general. The NW-/SE-trending post-gneissosity folds become tighter towards the margins of the dome (Fig. 3D). Extension lineations (and relatively infrequent parallel intrafolial fold hinges) also trend mainly NW–SE (Fig. 8).

The NW tip of the dome is an almost isoclinal neutral fold with both limbs dipping 60–75° SW and vertical gneissosity at the hinge. This fold is inter-

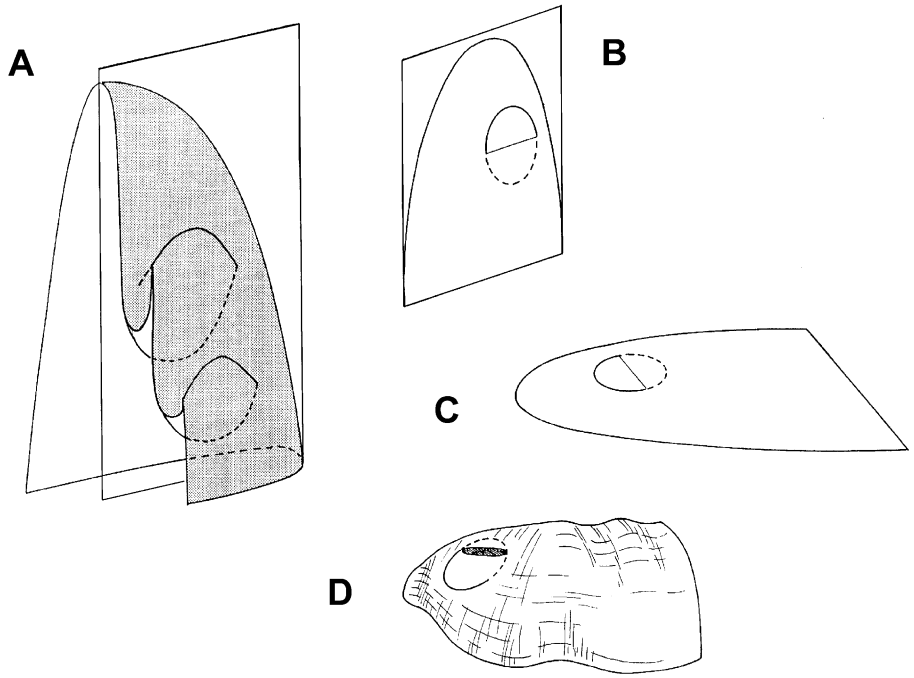

Fig. 13. Interpretation of the folds at the northwestern end of Dome D. A: Sketch of the geometry of sheathlike parasitic folds. The folds to the immediate north of the tip of Dome D are pictured to have this geometry. B: Simplification of the folds in A. Only the hinges and dominant fold axial plane are shown. The synformal hinge of the parasitic sheath fold is dotted. C: Same illustration as B but with a recumbent orientation, representing the northern end of the sheath fold of Dome D. D: Later folding of the sheath fold of Dome D also showing the origin of the small elliptical dome (shaded ellipse) north of the tip of Dome D, as an inverted synformal sheath.

preted to be the tip of a sheath fold, with axial plane tilted from an initially sub-horizontal orientation, to steeply SW dipping. This means that the northern margin of D, bordering domes B and C, is the lower limb of the sheath fold. The twisting rotation of the NW end of D (compared to the SE parts of the dome) is the result of the original sheath fold being pushed around the monoclinally folded pair of sheaths of domes B and C, as shown in Figs. 10B and 13D. These rotation effects terminate roughly at locations on the NE and SW margins of the dome where the gneissosity adopts approximately vertical dips. In the SE part of the dome, bounded NE and SW by these vertical margins, the sheath fold limbs were sub-horizontal before the NE-/SW-trending post-gneissosity folds. The evidence for this is the existence of the upright elliptical dome-and-basin structures described above, which are restricted to this SE half (see Fig. 14). The origin of the vertically dipping sides of dome D in this SE half will be explained below. The folds on the sheath lower limb of D (S of domes B and C) also probably formed during the pushing of the sheath of D over and around monoclinally folded sheaths of B and C. This may explain the spatial association of these folds on the lower limb with what appear to be fault dislocations of meta-gabbro lenses (or boudins) in the same area.

The flat top (upper enveloping surface of the dome-and-basins) of dome D and its sub-vertical NE and SW margins (seen in Figs. 4C and 11D) are explained as follows. For the sub-horizontal part of the sheath in the SE half of dome D, the sheath *y*-axis is sub-horizontal. Modest shortening in the NW–SE direction and later in the NE–SW direction produced gentle dome and basin structures, which have buckled the flat-lying gneissosities on the limbs of the sheath. Shortening along the NE–SW direction (the *y*-axis) is shown in Fig. 15B to also produce flattening of the sides of the sheath (and thereby increasing the area of vertical foliations along the sheath fold hinge).

Cross section D–D′ (Fig. 4C) shows the arching of the sheath of dome D partly over domes B and C and the internal buckling of the sheath in the SW part of the section. NE–SW shortening of the NW (previously tilted) end of the dome, has apparently only steepened the dip of the sheath here.

4.8. Structural interpretation of areas NW of domes B,C and D

Dome A was not examined in this study, however, details of the orientation of gneissosity in this structure have been presented by Rashwan (1991). We have modeled this dome as the refolded monoclinally buckled upper limb of a sheath fold, in accord with our model for the remaining four domes of the complex (Figs. 10 and 11A). The dome shape itself is probably a result of the combination of NE- and NW-trending post-gneissosity folds. The proposed monoclinal flexure in Fig. 11A explains the rapid steepening of the gneissosity to vertical orientations just south of the dome. NW-/SE-plunging extension lineations in this area, described by Abdel Khalek and Abdel Wahed (1983), are consistent with this model.

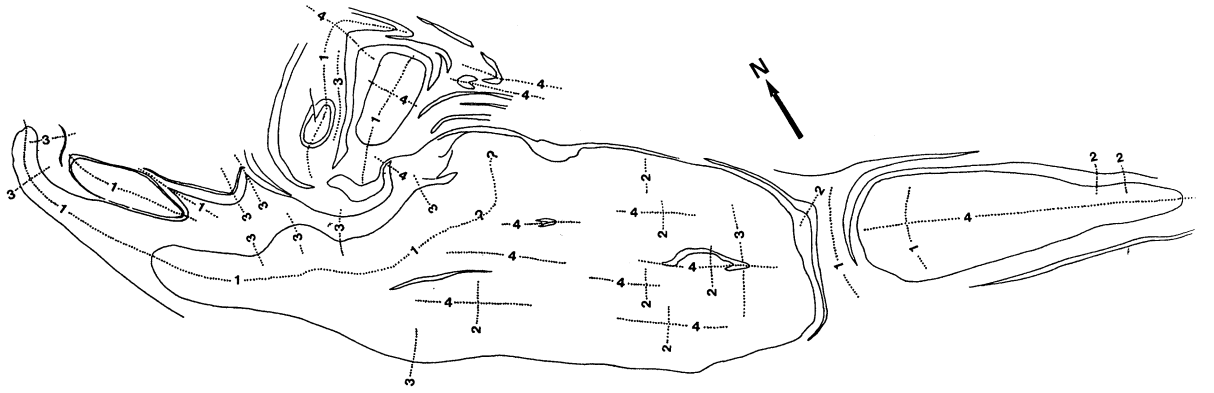

Fig. 14. Map of the Wadi Hafafit area showing the location of the axial planes of main macroscopic folds. 1=sheath fold axial planes. 2=NE-trending upright open folds; 3=monoclinal and associated folds; 4=N to NW-trending upright folds.

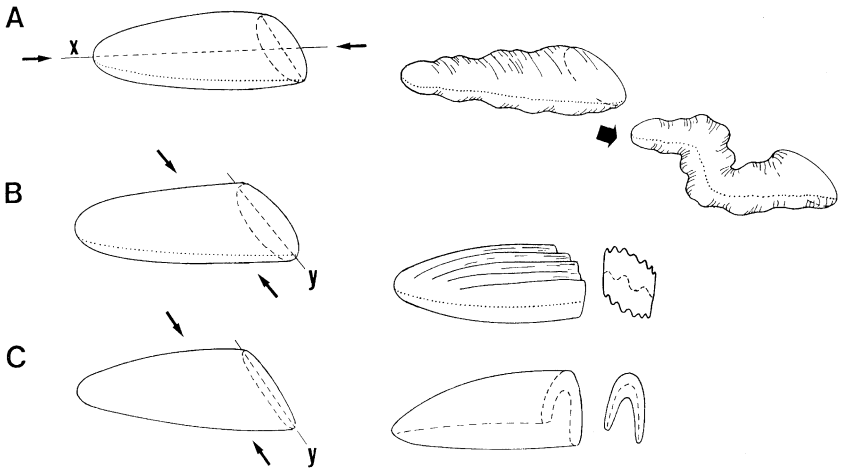

Fig. 15. Summary of the main styles of refolding of sheaths as expressed in the Wadi Hafafit area. A: Later shortening along the sheath *x*-axis leads to analogues of the NE-trending upright folds and later monoclinal flexures. B and C: Later shortening along the *y*-axis of the sheaths producing small-scale upright folds (analogous to the N–NW trending folds) or large scale flexures (analogous to the refolding of Dome B).

The tightly folded metasediments northwest of dome D were the subject of a study by Greiling et al. (1984), and require some re-interpretation. One of the most interesting features of this area is the presence of an elliptical isoclinal dome (2 km north of the granitoid gneiss-cored tip of dome D, Fig. 4B) with both limbs dipping about 50° SW. The northern tip of the dome dips 30° NW while its southern tip dips more than 50° SE. Close by and to the SW, NW and N of this isoclinal dome, lies a large fold with curved axial plane. This fold is the continuation of the sheath fold of dome D, and represents an outer sheath of meta-gabbro enclosed by metasediments. All of the sheaths so far described for domes B to E were originally antiformal. In this area northwest of dome D and in cross section A–A′ (Fig. 4C), it is clear that the antiformal sheaths have outermost layers of metasediment. Therefore, the elliptical isoclinal dome described above, being antiformal, is odd, as it is cored by metasediment. The curved extension of dome D sheath fold curving around the isoclinal dome is also odd, since the gneissosity dips at the tip of the folded meta-gabbros identify it as synformal, with an outer layering of metasediment. These two fold structures are explained in Fig. 13A–D as having been inverted (from synform to antiform and vice versa) as a result of bending of the sheath around domes B and C (see Section 3.6). The elliptical isoclinal dome was originally a sheath synform parasitic on the lower limb of the larger sheath of dome D, as shown in Fig. 13A. This synform was preserved, while others so far in the WHC have been flattened and sheared beyond recognition, probably due to the much stronger lithology represented by the metasediments in its core.

The location of the main macroscopic folds in the Wadi Hafafit area is presented in Fig. 14, where the main generations of folds are informally identified as sheath folds, NE-trending upright open folds, monoclinal and associated folds, and N–NW-trending upright folds.

5. Discussion

5.1. Comparison with earlier deformation schemes

A structural evolutionary scheme involving eleven deformation phases (D1 to D11) in the WHC was presented by El Ramly et al. (1984) and Greiling et al. (1984). It was later grouped into four deformation stages (D1–D4; D5–D7; D8–D10; D11) by El Ramly et al. (1993), and subsequently modified to nine deformation phases (Greiling et al., 1994). A problem with these schemes in their various forms is that orientation data (stereographic or map) for the structural elements of each were not presented in the original papers, and clear criteria for the recognition of these structures was also not available. We recom-

mend a full reappraisal of the existing schemes of deformation phases and their terminology, in the light of the discovery of sheath folds in this area. A brief comparison of the structures found in this study with that of El Ramly et al. (1993) is presented below and in Table 1.

The first stage (D1 to D4) included the development of the gneissosity and isoclinal intrafolial folds. The separation of each phase D1 to D4 was based on the observation that S1-foliated inclusions occurred in gabbro; the gabbro was itself S2-foliated and occurred as an inclusion in diorite; the diorite was itself S3-foliated, and so on (El Ramly et al., 1984; Rashwan, 1991). This evidence is also consistent with syn-kinematic intrusions in a single deformation episode, and this is the interpretation we prefer. This stage is also the time of development of the macroscopic sheath folds, because the sheaths are synchronous with extreme extension, which produced mineral lineations, which are developed on gneissosity planes and are defined by the same minerals as the gneissosity. At this time, banding and boudinage developed parallel to the gneissosity, enhancing and complicating the appearance of this foliation. The banding is probably an effect of extreme flattening and stretching of contrasting lithologies, e.g. minor dykes, xenoliths, etc., and may constitute a transposed layering.

The D5 early mylonitic shears of El Ramly et al.'s (1993) scheme, are identified here as numerous local mylonite zones with high-temperature mineralogy, especially in the metagabbros. These shears probably also belong in the sheath folding stage, because the mylonites are isoclinally folded about gneissosity-parallel axial planes.

D6 folds with NE–SW general trends may comfortably be identified as the open upright NE-/SW-trending post-gneissosity folds, which preceded monoclinal folding in the WHC. The NE-trending monoclinal folds were not included in El Ramly et al.'s (1993) scheme in this stage. The latter authors describe D7 drag folds, which were associated with SW-/WSW-ward D8 thrusting of the Wadi Ghadir

Table 1
Correlation of the sequence of structural and intrusive events for the Migif–Hafafit Gneissic Complex, as determined by this study, with the deformation schemes presented by Greiling et al. (1984), El Ramly et al. (1993) and Greiling et al. (1994)

Greiling et al. (1984), El-Ramly et al. (1993)			Greiling et al. (1994)			This study
"Early deformation"	D1	planar fabric	Phase 1	D1	planar fabric	progressively more silicic calc-alkaline syn-kinematic intrusions gneissosity and lineations isoclinal folds, macroscopic sheath folds mylonites
	D2	metamorphic banding, migmatization		D2	metamorphic banding, migmatization	
	D3	foliation, isoclinal folds		D3	foliation, isoclinal folds	
	D4	foliation, isoclinal folds	Phases 2, 3	D4	foliation, isoclinal folds	
"Early thrusting and folding"	D5	mylonites		D5	mylonites	
	D6	NE–SW trending fault bend folds		D6	NE–SW trending open folds	NE–SW trending upright open folds
						macroscopic monoclinal folds
	D7	drag folds	Phase 4	D7	drag folds	thrusting
"Regional thrusting and folding"	D8	thrusting		D8	thrusting mylonites fault bend folds	
	D9	chevron folds				
	D10	NW–SE trending open folds				NW–SE trending upright folds
"Gravitative uplift"	D11	open folds, flat-lying axial surfaces		D9	open folds, flat-lying axial surfaces	not present

Deformation phases 1, 2, 3, 4 refer to phases of tectonic evolution of mountain belts as outlined by Dewey (1988).

ophiolites over the WHC (El Bayoumi and Greiling, 1984; Greiling et al., 1984, 1988) to be followed by local D9 chevrons and D10 NW–SE-trending macroscopic folds. In later modifications the SW-ward thrusting of the Wadi Ghadir ophiolite was re-interpreted as NW-ward thrusting (Greiling et al., 1993), and the NW–SE-trending folds were identified as ramp antiforms above lateral ramps, and as NE–SW-trending folds and monoclines. The existence of the ramp-related antiforms in these latter model is discussed later. The evidence for and against the last event (D11 of El Ramly et al., 1993) is now considered.

5.2. The status of gravitative uplift of domes in the WHC

Gravitative uplift has been proposed in many publications on the WHC, without firm evidence. The suggested evidence for a steep stress field (associated with gravitative uplift) was the presence of gently inclined to recumbent open folds (e.g. Fig. 3E) in some areas of the WHC (Greiling et al., 1984). This is a misinterpretation of the effects of later monoclinal folding of post-gneissosity upright NE-trending folds. The NE-trending folds were rotated along with the gneissosity as shown in Fig. 9D.

Other features of the WHC that have been presented in favour of gravitative uplift of the domes include: (a) the central parts of the domes are occupied by later intruded, less deformed granitoid material (El Ramly et al., 1984); (b) the WHC shows a regional plunge reversal (from NW-wards in the NW to SE-wards in the SE) with the largest dome D near the centre; (c) other smaller fold plunge reversals; (d) ‘‘disharmonic’’ folding in the domes (including the obscuring of synforms); (e) peculiar dome shapes and dip variations along the dome margins.

The first point (a) is disputed in this study. There is no evidence that there is significantly less deformation in the centres of domes B to E. All units in these domes show the full range of structures from gneissosity of post-gneissosity folding, hence, all units were emplaced before the end of gneissosity development. The centre of dome C is occupied by a trondjhemite with a low mafic mineral content. For this reason the gneissosity and lineations are less obvious, but they are still present. Intrafolial folds are isoclinal in the centre of these domes as they are in places away from the centres (e.g. Fig. 3A). If gravitative uplift were a late stage event (D11 in Greiling et al., 1984), there is no evidence for distortion of fold and lineation trends that should accompany it. The curved mineral lineation trends, so well developed in domes B and C, cannot be the result of gravitative distortion, because these lineations formed during gneissosity development, at which time the gneissosity outlined low-dipping sheath fold structures. Therefore the strain affecting these lineations occurred within sub-horizontal planes—and this is not a characteristic of gravitative uplift. Also, there is the evidence of curved lineations observed directly on planar gneissosity surfaces.

Regarding point (b), the WHC forms a narrow NW-trending zone enclosing the domes A to E. It is unavoidable that the NW end will plunge NW and SE end will plunge SE in such an arrangement, therefore this feature has little significance for the macroscopic structure of the WHC. Dome D is largest because the sheaths A, B and C lie below it, and are therefore less exposed. Dome E lies above D, but is located just SE of a monoclinal flexure, which has lifted the SW end of dome D relative to dome E. Most of the other folds with curved hinges (point c) would require an inclined direction of proposed uplift. Evidence (d) is a characteristic of sheath folds, not of gravitative uplift. The dips at the margins and shapes of the domes (point e) are best explained by fold interference patterns described above in Sections 4.5–4.8.

5.3. The antiformal duplex model of the WHC

The Nugrus Thrust, bounding the WHC to the north, is a major low-dipping shear zone with hanging wall displaced to the NW, and separates tier 1 gneissic rocks from tier 2 low-grade upper crustal rocks (Greiling et al., 1996; Greiling, 1997). It has been further proposed that the WHC beneath the Nugrus Thrust forms the lower element of an antiformal stack formed at the time of thrusting of the Nugrus (D8 in El Ramly et al., 1993). The WHC in this model is a ‘‘horse’’ bounded above by the Wadi Gemal Thrust, and below by the Migif–Hafafit Thrust—a thrust projected under the WHC from exposures 25 km to the west (Greiling et al., 1993; Greiling, 1997). In concert with this model, the WHC fold interference pattern has been interpreted to be partly composed of

large-scale fault bend folds, including monoclines, foot wall antiforms and hanging wall antiforms, associated with ramps in the Migif–Hafafit Thrust (Greiling, 1997; Greiling et al., 1988, 1996).

The folds previously suggested to be ramp-related antiforms are (a) a NW-trending fold occupying the length of the WHC from SE to NW; (b) a second antiform meeting the first at the SE end of the WHC and diverging northwards, and (c) a third NE–SW-trending hanging wall antiform just SE of the Nugrus Thrust near Gebel Migif (Greiling et al., 1988; Greiling and Rashwan, 1994; Greiling, 1997). None of these interpreted antiforms is correct. With respect to (a), dome D does not contain the discrete antiform suggested by Greiling (1997)—in the SE half of the dome there are numerous NW-/SE-trending post-gneissosity antiforms and synforms without any being the dominant fold. They are confined to that part of the original sheath which had sub-horizontal limbs before the final NE–SW shortening. These post-gneissosity folds fade to the NW at the same place where turning of the sheath to SW dips in its NW half has allowed the sheath axial plane to crop out. This latter antiform is an earlier generation to the antiforms farther SW. Similarly with (b), there is no evidence for antiformal closure at all along this trend except perhaps in the vicinity of domes B and C. The antiform proposed for (c) is not supported by gneissosity orientations. In short, the entire concept of ramps in the hypothetical Migif–Hafafit thrust is not supported by the field evidence.

5.4. Characteristics of refolding of sheath folds in the WHC

The refolding of the sheath folds of the WHC has first involved shortening along their *x*-axis followed by shortening along their *y*-axis. Both shortening events reveal interesting deformation behaviour of sheath folds. The shortening along the *x*-axis of the sheaths initially produced open (NE-/SW-trending) folds in the low-curvature limbs of the sheaths (Fig. 15A). The tighter curvature of the sheath hinges, wrapping around the limbs of the fold, resists this small wavelength folding, with the result that the dome margins are generally smoothly curved. This resistance may also explain why the NE-/SW-trending post-gneissosity folds were succeeded by larger scale widely spaced monoclines, which affect the entire sheath rather than local parts of the limbs (Fig. 15A). This monoclinal style of folding has an analogue in the buckling of a cigarette when it is stubbed—small wavelength folding is resisted in favour of large amplitude deflections.

During the later shortening of the sheath folds, along their *y*-axes, the ellipticity of the cross section of the sheath appears to control the characteristics of the refolding. If this ellipticity (*y*/*z* ratio) is large, then the sheath buckles after a style similar to type-2 refolding, where the axial plane buckles (Fig. 15C). This appears to have occurred in the case of dome B (Fig. 11B), and similar sheath refolding has been illustrated by Henderson (1981). If the *y*/*z* ratio is lower, then a type-1 refolding style appears to be preferred. For the sheaths like this, the elliptical cross section becomes deformed as if it were a strain ellipse, and a lower *y*/*z* ratio results (Fig. 15B). This is apparently the deformation response of the sheaths of Domes C, D and E. This style of refolding of a sheath is well expressed in Dome D (cross section C–C′ in Fig. 4C). In this cross section and on Fig. 4A, it is clear that Dome D is bounded to the NE and SW by vertical flanks. Fig. 15B demonstrates that even modest shortening along the sheath *y*-axis is sufficient to produce such an isoclinal dome. Modest shortening is consistent with the NW–SE-trending open folding of the upper surface of the dome.

The divergent refolding behaviour of sheaths shortened along the *y*-axis may be compared with the refold mechanisms described by Julivert and Marcos (1973), where the first generation fold interlimb angle determined whether type 1 or 2 interference occurred in refolds. The *y*/*z* ratio of the sheath is related to the sheath interlimb angle, hence dome B, with smaller interlimb angle has refolded in a manner similar to type 2 fold interference patterns, whereas dome C, with larger interlimb angle, has refolded like type 1. The type of sheath refolding shown in Fig. 15B involves only modest distortion of the upper limbs of the sheath, explaining why sheath fold-related extension lineation trends were preserved in domes B and C, for example.

The conclusion that the peculiar fold interference pattern shown by the gneiss-cored domes of the WHC is a result of refolding of early macroscopic sheath folds may assist the recognition of these folds in other

gneissic terrains. The repertoire of refolding styles of sheaths seems limited by the girdling effect of the strongly curved fold hinge. Thus, similar patterns may be expected elsewhere in these terrains. Clues as to the original shape, e.g. y/z ratio of the sheaths may also be provided by the style of the refolds.

Acknowledgements

The authors dedicate this work to M.F. El-Ramly, and thank him for his encouragement, inspiration and insight, without which this project would not be possible. The authors thankfully acknowledge the contribution by Mr Abdel-Monem Mohammed Soltan during the field mapping of the WHC. We appreciate the logistical assistance of Mr. Ahmed Mahmoud Badawy at EGSMA and Mr Mahmoud Saeed Gaad Al Kareem at Marsa Alam. The thoughtful comments of Haakon Fossen and Kip Hodges have contributed to the improvement of the manuscript.

References

Abdel Khalek, M.L., Abdel Wahed, M., 1983. Structural setting of the Hafafit gneisses, Eastern Desert, Egypt. Abstr. 5th Int. Conf. Basement Tectonics, Cairo, Egypt, 8.

Bennett, J.D., Mosley, P.N., 1987. Tiered tectonics and evolution, Eastern Desert and Sinai, Egypt. In: Matheis, Schandelmeier (Eds.), Current Research in African Earth Sciences. Balkema, Rotterdam, pp. 79–82.

Cobbold, P.R., Quinquis, H., 1980. Development of sheath folds in shear regimes. J. Struct. Geol. 2, 119–126.

Dewey, J.F., 1988. Extensional collapse of orogens. Tectonics 7, 1123–1139.

El Bayoumi, R.M.A., Greiling, R., 1984. Tectonic evolution of a Pan-African plate margin in southeastern Egypt—a suture zone overprinted by low angle thrusting? In: Klerkx, J., Michot, J. (Eds.), African Geology, Tervuren, pp. 47–56.

El Gaby, S., El Nady, O., Khudeir, A., 1984. Tectonic evolution of the basement complex in the central Eastern Desert of Egypt. Geol. Rundsch. 73, 1019–1036.

El Gaby, S., List, F.K., Tehrani, R., 1988. Geology, evolution and metallogenesis of the Pan-African belt in Egypt. In: El Gaby, S., Greiling, R.O. (Eds.), The Pan-African Belt of Northeast Africa and Adjacent Areas. Vieweg and Sohn, Weisbaden, pp. 17–68.

El Ramly, M.F., Akaad, M.K., 1960. The basement complex in the central Eastern Desert of Egypt between latitudes 24°30′ and 25°40′N. Geol. Surv. Miner. Res. Dep., Egypt, Pap. 8, 35 p.

El Ramly, M.F., Greiling, R.O., 1988. Wadi Hafafit Area—1:100,000 Geology Map. Technische Fachhochschule, Berlin.

El Ramly, M.F., Saleeb Roufaiel, G.S., 1974. Sodic silica metasomatism and introduced zircon in the Migif Hafafit gneisses, Eastern Desert. Egypt. J. Geol. 18, 119–126.

El Ramly, M.F., Greiling, R., Kröner, A., Rashwan, A.A.A., 1984. On the tectonic evolution of the Wadi Hafafit area and environs, Eastern Desert of Egypt. Bull. Fac. Earth Sci. King Abdulaziz Univ. 6, 114–126.

El Ramly, M.F., Greiling, R., Rashwan, A.A., Rasmy, A.H., 1993. Explanatory note to accompany the geological and structural maps of Wadi Hafafit area, Eastern Desert of Egypt. Geol. Surv. Egypt, Pap. 68, 53 p.

Ghosh, S.K., 1993. Structural Geology: Fundamentals and Modern Developments. Pergamon, Oxford, 598 p.

Goscombe, B., 1991. Intense non-coaxial shear and the development of mega-scale sheath folds in the Arunta Block, Central Australia. J. Struct. Geol. 13, 299–318.

Greiling, R.O., 1997. Thrust tectonics in crystalline domains: the origin of a gneiss dome. Proc. Indian Acad. Sci. 106, 209–220.

Greiling, R.O., El Ramly, M.F., 1990. Wadi Hafafit Area—Structural Geology 1:100,000. Technische Fachhochschule, Berlin.

Greiling, R.O., Rashwan, A.A., 1994. Large-scale shear-zones and related mineral deposits: examples from the Nubian Shield (Proterozoic Egypt). Africa Geosci. Rev. 1, 503–514.

Greiling, R.O., Kröner, A., El Ramly, M.F., 1984. Structural interference patterns and their origin in the Pan-African basement of the southeastern desert of Egypt. In: Kröner, A., Greiling, R. (Eds.), Precambrian Tectonics Illustrated. E. Schweizerbart'sche Verlagsbuchhandlung, Stuttgart, pp. 401–412.

Greiling, R.O., Kröner, A., El Ramly, M.F., Rashwan, A.A., 1988. Structural relationships between the southern and central parts of the Eastern Desert of Egypt: details of a fold and thrust belt. In: El Gaby, S., Greiling, R.O. (Eds.), The Pan-African Belt of Northeast Africa and Adjacent Areas. Vieweg and Sohn, Weisbaden, pp. 121–145.

Greiling, R.O., Rashwan, A.A., El Ramly, M.F., Kamal El Din, G.M., 1993. Towards a comprehensive structural synthesis of the (Proterozoic) Arabian–Nubian Shield in E. Egypt. In: Thorweihe, Schandelmeier, (Eds.), Geoscientific Research in Northeast Africa. Balkema, Rotterdam, pp. 15–19.

Greiling, R.O., Abdeen, M.M., Dardir, A.A., El Akhal, H., El Ramly, M.F., Kamal El Din, G.M., Osman, A.F., Rashwan, A.A., Rice, A.H.N., Sadek, M.F., 1994. A structural synthesis of the proterozoic Arabian–Nubian shield in Egypt. Geol. Rundsch. 83, 484–501.

Greiling, R.O., de Wall, H., Warr, L.N., Naim, G.M., Hussein, A.A., Sadek, M.F., Abdeen, M.M., El Kady, M.F., Makhlouf, A., 1996. Basement structure in Eastern Egypt: quantitative perspectives for the second century. Proc. Geol. Surv. Egypt Cenn. Conf., 289–302.

Hedge, C.E., Stern, R.J., Davis, F.B., 1982. Geochronology of basement rocks along the northern Red Sea. Precambrian Res. 16, A23–A24.

Henderson, J.R., 1981. Structural analysis of sheath folds with horizontal X-axes, northeast Canada. J. Struct. Geol. 3, 203–210.

Julivert, M., Marcos, A., 1973. Superimposed folding under flexural conditions in the Cantabrian Zone (Hercynian Cordillera, northwest Spain). Am. J. Sci. 273, 353–375.

Kröner, A., Reischmann, T., Wust, H.-J., Rashwan, A.A., 1988. Is there any Pre-Pan-African (>950 Ma) basement in the Eastern Desert of Egypt? In: El Gaby, S., Greiling, R.O. (Eds.), The Pan-African Belt of Northeast Africa and Adjacent Areas. Vieweg and Sohn, Weisbaden, pp. 95–119.

Kröner, A., Krüger, J., Rashwan, A.A.A., 1994. Age and tectonic setting of granitoid gneisses in the Eastern Desert of Egypt and south-west Sinai. Geol. Rundsch. 83, 502–513.

Lacassin, R., Mattauer, M., 1985. Kilometre-scale sheath fold at Mattmark and implications for transport direction in the Alps. Nature 315, 739–742.

Rashwan, A.A., 1991. Petrography, geochemistry and petrogenesis of the Migif–Hafafit gneisses at Hafafit mine area, Egypt. Sci. Ser. Int. Bur., vol. 5. Forschungszentrum Julich, 359 p.

Rhodes, S., Gayer, R.A., 1977. Non-cylindrical folds, linear structures in the X direction and mylonite developed during translation of the Caledonian Kalak Nappe Complex of Finnmark. Geol. Mag. 114, 329–408.

Skjernaa, L., 1989. Tubular folds and sheath folds: definitions and conceptual models for their development, with examples from the Grapesvare area, northern Sweden. J. Struct. Geol. 11, 689–703.

Vollmer, F.W., 1988. A computer model of sheath-nappes formed during crustal shear in the Western Gneiss Region, central Norwegian Caledonides. J. Struct. Geol. 10, 735–743.

Williams, G.D., Chapman, T.J., 1979. The geometrical classification of non-cylindrical folds. J. Struct. Geol. 1, 181–185.